University of Tasmania
Department of Civil and Mechanical Engineering

Honours Thesis # 96/3

VELOCITY DISTRIBUTIONS WITHIN AN UNDULAR HYDRAULIC JUMP

This thesis is submitted in partial fulfillment of the requirements of Bachelor of Engineering with Honours

Robert Dunbabin

November 1996

Use of Thesis

This thesis contains no material which has been accepted for the award of any other degree or diploma in any university. To the best of my knowledge, this thesis contains no copy or paraphrasing of material previously published except where due reference has been made in the text.

Abstract

The investigation of undular hydraulic jumps is a relatively new field of study. The phenomenon is characterised by three-dimensional flow patterns, non-hydrostatic pressures and cross channel shock waves. To date, few detailed study of the velocity profiles has been undertaken. The aim of this project was to give some insight into the flow regime by measuring and analysing velocity profiles on the centre-line of the jump.

It was discovered that the velocity profiles followed the accepted theories of turbulent boundary layer flow with respect to the law of the wall and Coles' law of the wake. Many similarities were found between the wake term for this work and other recorded studies of flows with high longitudinal pressure gradients. A new and apparently universal relationship was found between Coles' Π and the non-dimensionalised pressure gradient, β for many different flow regimes. This was of the form $\Pi = 0.246\ \beta^{0.431}$ and applied to flows such as diffusers, aero-foils, cylinders and steps as well as the undular hydraulic jump.

Acknowledgments

Many thanks must go to Dr. Sergio Montes for his continual input and help throughout this honours project. From the time he suggested the topic, he has always been keen to help with all aspects of the project, suggesting references and increasing greatly my knowledge in the area of fluid mechanics.

The time spent by my Mother and Father has been greatly appreciated.

I would also like to thank Matthew and Vanessa for their contribution.

Index

1 Notation

Symbol	S.I. Units	Definition
A	m^2	cross-sectional area of the channel
		A=b*D
or	[-]	constant
B	[-]	constant
b	m	channel width
C_1	[-]	constant
C_2	[-]	constant
c_f	[-]	local skin friction coefficient
		$c_f = 2\left(\frac{v^*}{U_{max}}\right)^2$
D	m	total depth of water
d	m	diameter of pitot tube (for Preston tube)
d_c	m	critical depth
		$d_c = \sqrt[3]{\frac{q^2}{g}}$ for a rectangular channel
Fr	[-]	Froude number
		$Fr = \frac{q}{\sqrt{gD^3}}$ for a rectangular channel
f	[-]	channel friction factor
$f\left(\frac{yv^*}{\nu}\right)$	[function]	part of the law of the wall
g	m/s^2	acceleration due to gravity
		g = 9.8044 in Hobart, Tasmania

$g\left(\Pi,\frac{y}{\delta}\right)$	[function]	part of the law of the wake
H_{static}	m of water	static head
H_{total}	m of water	total head
h	m	head of water over V-notch weir
P	m of water	static pressure head (for Preston tube)
P_w	m	perimeter of wetted surface of channel
p	Pa	pressure
p_0	m of water	total pressure head (for Preston tube)
Q	m^3/s	volumetric flow rate
q	m^2/s	flow per unit width
R	m	hydraulic radius $R=A/P_w$
S_0	[-]	Channel slope
t	°C	water temperature
U	m/s	average velocity at a section
U_{max}	m/s	maximum point velocity
v	m/s	fluid velocity measured parallel to the channel bottom
v_c	m/s	critical velocity
v*	m/s	friction velocity $v^* = \sqrt{\frac{\tau_0}{\rho}}$
x	m	distance measured laterally along the channel
y	m	distance to the channel bed, measured vertically
y_c	m	critical depth

		$y_c = \sqrt[3]{\frac{Q^2}{gb^2}}$ for a rectangular channel
z_{datum}	m	vertical height measured from datum
β	[-]	non-dimensional longitudinal pressure gradient
γ	kg/m^2s^2	specific weight of water
		$\gamma = \rho g$
δ	m	depth of maximum velocity from channel bottom
κ	[-]	constant
ν	m^2/s	kinematic viscosity
ν_t	m^2/s	turbulent eddy viscosity
Π	[-]	Coles' wake parameter
ρ	kg/m^3	density
		$\rho = 1000$ for water
τ_0	kg/ms^2	local skin friction
$\omega\left(\frac{y}{\delta}\right)$	[function]	Coles' wake function

2 Introduction

2.1 The Hydraulic Jump

Water flowing in open channels can make a transition from a fast, shallow state to a deeper, slower state. This transition is called a hydraulic jump and is illustrated in Figure 2.1.1. The phenomenon usually involves an extremely turbulent region of flow recirculation, called a roller, which is characterised by air entrainment, waves and spray. Associated with the turbulence are energy losses and much mixing occurs in this region. The length over which the hydraulic jump occurs is commonly between four and six times the downstream channel depth (Gerhart and Gross [8]).

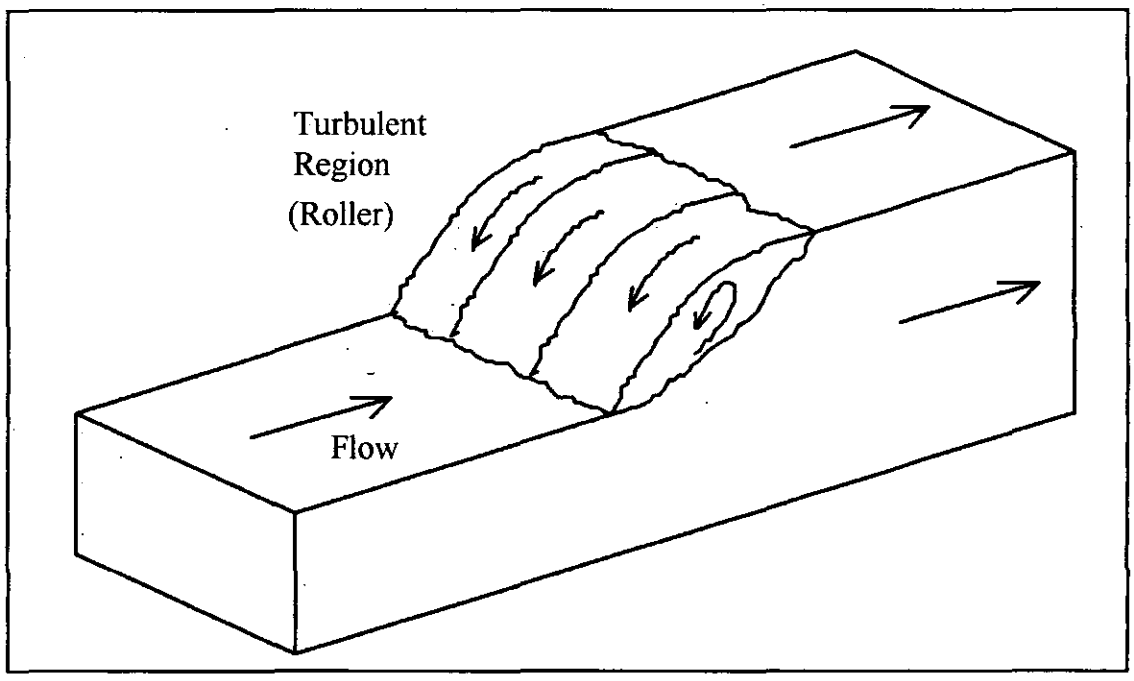

Figure 2.1.1- Schematic of a hydraulic jump

2.2 The Undular Hydraulic Jump

According to Chanson [3], the hydraulic jump changes form when the upstream depth is close to the critical depth of the channel (the critical depth is that depth where the flow has the minimum specific energy). When this occurs,

the effects of the jump are no longer confined to a small region of the channel, but standing waves are formed on the surface, which can propagate downstream for more than ten wavelengths.

Chanson [3] found that unlike regular hydraulic jumps, the undular hydraulic jump exhibits three dimensional flow patterns, with cross-channel shock waves initiating from the sidewalls. He describes relationships between the wavelength, angle of cross-channel shock waves, height of the first crest, propagation of waves and the upstream Froude number. A schematic drawing of an undular jump, showing the first one and a half undulations is shown in Figure 2.2.1. Labeled on this sketch are the position of the crests, troughs, shock waves and a small roller at the first crest. A side view of the jump has been included in Figure 2.2.2 showing the first three waves.

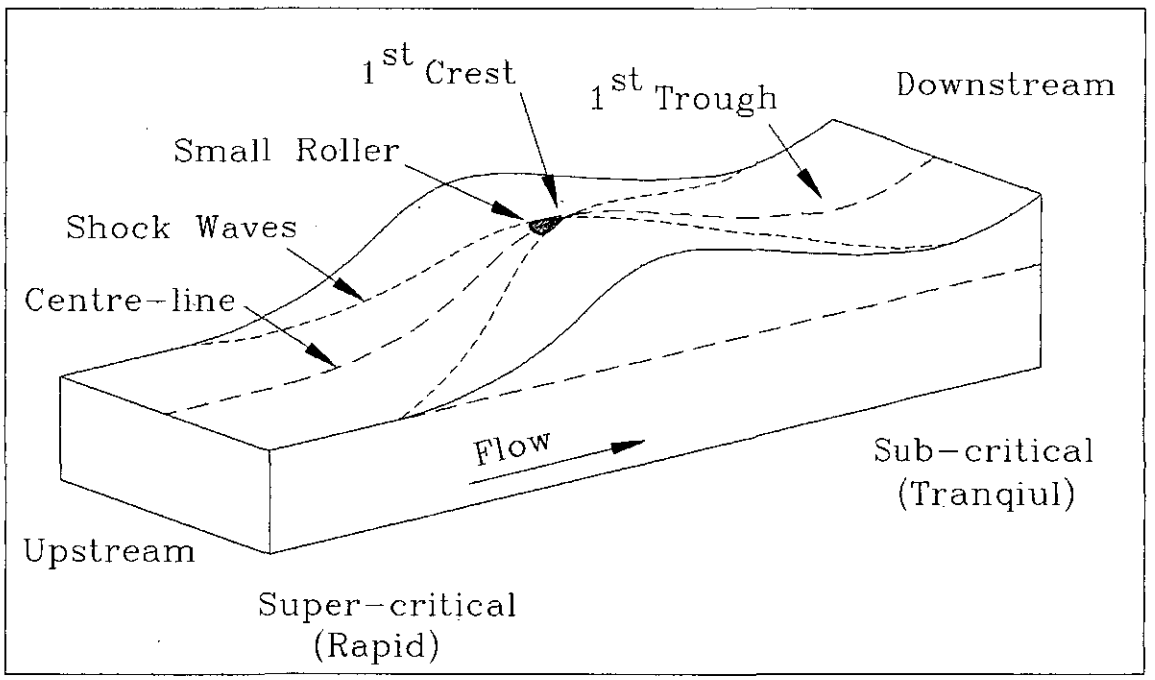

Figure 2.2.1- Schematic of an Undular Hydraulic Jump from an oblique perspective

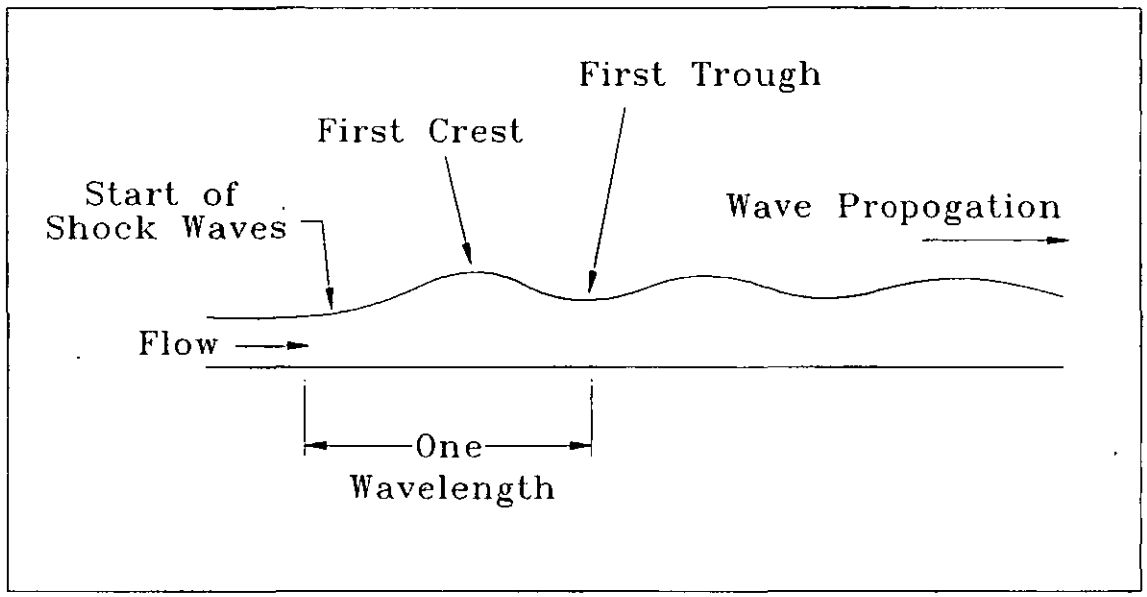

Figure 2.2.2 - Side View of an Undular Hydraulic Jump

Undular hydraulic jumps can occur in irrigation and water supply channels, shallow straights subjected to strong currents and natural rivers in tidal situations (Chanson [3]). He stressed that the effects of undular hydraulic jumps need to be seriously considered by channel designers. The waves propagating downstream may cause overtopping of banks in natural channels, causing erosion and possibly failure. The waves may also cause increased fatigue loading on downstream canal control structures such as gates and weirs. The adverse effects of the waves on pumps and flow measurement devices also needs to be considered.

2.3 Investigation

Few detailed analyses of the velocity profiles throughout the undular hydraulic jump have previously been undertaken. There is no accurate theory available for predicting where undular hydraulic jumps will form. Methods used for regular hydraulic jumps, such as those indicated in Duncan, Thom and Young [7], are not particularly suited because of the propagation of the waves downstream. One of the aims of this thesis was to study the flow velocities, in order to give an insight into the flow mechanisms within the undular hydraulic jump, hopefully to provide material from which accurate predictive analysis could be undertaken.

The experiments were also designed to examine any longitudinal pressure gradients and the amount of mixing taking place, both of which have received scant attention in the study of the undular hydraulic jump.

It was hoped that the results from the analysis could be used to compare the undular hydraulic jump to other flow situations. For this purpose, a substantial amount of data published in the proceedings for the conference on 'Computation of Turbulent Boundary Layers' at Stanford in 1968 [6] was used. Over one hundred experiments similar to the current work were presented, however in general, the flow conditions which were investigated were different. Included were cases of longitudinal pressure gradients in such as diverging channels, flow over steps, flow around aero-foils, flow though air diffusers, flow along cylinders and cases of forced mixing. The data had been used for testing computational theories for predicting the velocity distributions and boundary layer development, but the raw data included was an excellent source for comparison.

Among the few works of this nature in open channel flow, one may quote the paper by Kironoto and Graf [9], where the effects of longnitudal pressure gradients on velocity profiles in accelerating and decelerating flows. It was also intended to compare results gained from the current experiments to these other investigations.

2.4 Project Aims

A short summary of the aims of the project has been included below:

- Carry out a detailed study of the velocity distributions within the jump.
- Investigate any longitudinal pressure gradients.
- Study the distribution of eddy viscosity, which is an indication of the amount of mixing taking place, throughout the jump.
- Compare present results to previous studies of undular hydraulic jumps by Chanson [3].
- Compare the velocity distributions to data published by Coles and Hirst [6] and Kironoto and Graf [9].
- Provide an insight into the flow mechanisms taking place in the undular hydraulic jump.

3 Theory

3.1 Open Channel Flow

A hydraulic jump is observed when channel flow makes a transition from fast and shallow to slow and deep. The jump effectively divides the flow between the two states. In open channels, the state of the flow can be described by its average specific energy over a given cross section. When the specific energy is at a minimum, critical flow conditions are said to exist. The depth and velocity under these conditions are called the critical depth and critical velocity respectively. For a rectangular channel of width b and flow rate Q, the following relationships exist (Gerhart and Gross [8]):

$$\text{critical depth,} \qquad y_c = \sqrt[3]{\frac{Q^2}{gb^2}} \tag{3.1.1}$$

$$\text{critical velocity,} \qquad v_c = \sqrt{gy_c} \tag{3.1.2}$$

Flows with an overall depth $D < y_c$ have an average velocity $U > v_c$ and are called super-critical. Similarly, where $D > y_c$ (and $U < v_c$) the flow is sub-critical.

Hydraulic jumps become undular when the upstream Froude number, Fr is between 1.1 and 2.5 (Chanson [3]). The Froude number can be defined (Gerhart and Gross [8]) as the ratio between the average flow velocity, U and the small wave or ripple velocity, $v_w = \sqrt{gD}$,

$$\begin{aligned} Fr &= \frac{U}{v_w} \\ &= \frac{U}{\sqrt{gD}} \end{aligned} \tag{3.1.3}$$

and using the relation $U = \frac{q}{D}$,

$$Fr = \frac{q}{\sqrt{gD^3}} \tag{3.1.4}$$

Hence, for critical flow, Fr = 1, super-critical flow Fr > 1 and sub-critical flow Fr < 1.

3.2 Turbulent boundary layers

Analysis of the velocity profiles within the undular hydraulic jump requires an understanding of the currently accepted theories of the flow mechanisms in the layer near the channel wall, called the boundary layer. A turbulent flow is described in Schubauer and Tchen [12] as one where flow parameters such as velocities and pressures fluctuate with time about a mean value.

Most commonly, non-dimensionalised velocity information is displayed by plotting the parameter yv^*/ν on the horizontal axis and the parameter $\frac{v}{v^*}$ on the vertical axis (Prandtl [10]). Because of the large range in values of $\frac{yv^*}{\nu}$, this axis is plotted on a logarithmic scale. The transformation of data to this form involves the friction velocity, v^*, defined as:

$$v^* = \sqrt{\frac{\tau_0}{\rho}} \tag{3.2.1}$$

This is an indication of the effect of the shear effects of the wall on the fluid. A typical example of a plot showing some experimental values for uniform flow is shown in Figure 3.2.1.

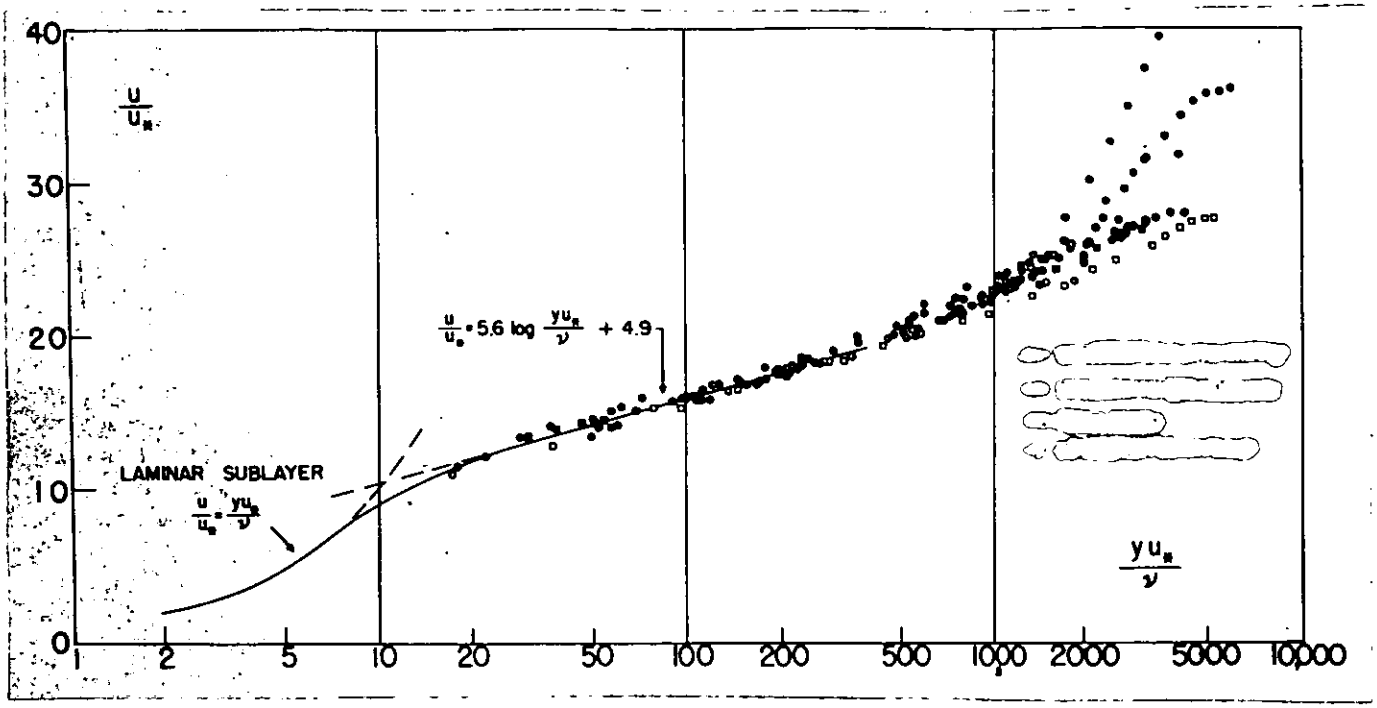

Figure 3.2.1- Universal Velocity Distribution for Turbulent Velocity Profilesnear Smooth Walls - Clauser [4] pp. 95

According to Clauser [4], for lower values of $\frac{yv^*}{\nu}$, in the laminar sublayer, a linear relationship holds,

$$\frac{v}{v^*} = \frac{yv^*}{\nu} \tag{3.2.3}$$

whilst in the actual turbulent layer, a universal law called the law of the wall holds, where there is a logarithmic relationship between $\frac{v}{v^*}$ and $\frac{yv^*}{\nu}$:

$$\frac{v}{v^*} = A\log\left(\frac{yv^*}{\nu}\right) + B \tag{3.2.4}$$

For turbulent boundary layers with pressure gradients, measurements at large values of $\frac{yv^*}{\nu}$ show a deviation from the universal law. This deviation was first quantified by Coles [5], who proposed an extension to the law of the wall which he called the "law of the wake". The general form of this is:

$$\frac{v}{v^*} = f\left(\frac{yv^*}{\nu}\right) + g\left(\Pi, \frac{y}{\delta}\right) \tag{3.2.5}$$

where the function $g\left(\Pi, \frac{y}{\delta}\right)$ represents the deviation from the logarithmic law. To include the effects of any pressure gradients, this deviation function, or wake term, was written as a product function

$$g\left(\Pi, \frac{y}{\delta}\right) = \frac{\Pi(x)}{\kappa}\omega\left(\frac{y}{\delta}\right) \tag{3.2.6}$$

where the term $\Pi(x)$ is a function of x and is related to the pressure gradient, $\omega\left(\frac{y}{\delta}\right)$ is a universal wake term and κ is a constant. By analysing existing experimental data and using the normalising conditions $\omega(0) = 0$, $\omega(1) = 2$, and $\int_0^2 \left(\frac{y}{\delta}\right) d\omega = 1$, Coles [5] found the function ω had the form shown in Figure 3.2.2, which can be approximated by the equation

$$\omega = \sin^2\left(\frac{\pi}{2}\frac{y}{\delta}\right) \tag{3.2.7}$$

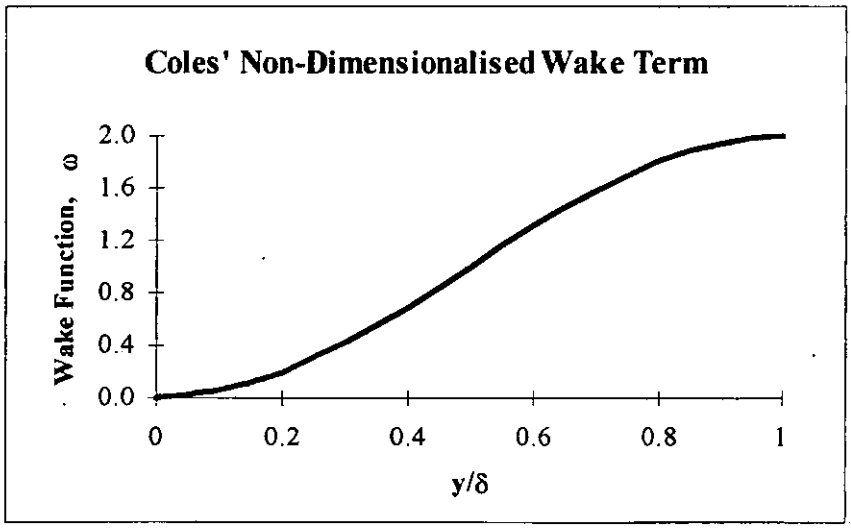

Figure 3.2.2- Coles' Wake Function, $\omega\left(\frac{y}{\delta}\right)$

An illustration (as drawn by Coles [5]) of the components f (wall) and g (wake) of equation 3.2.5 for the velocity porfile is included in Figure 3.2.3. The sum of the wall and wake components make up the overall velocity profile.

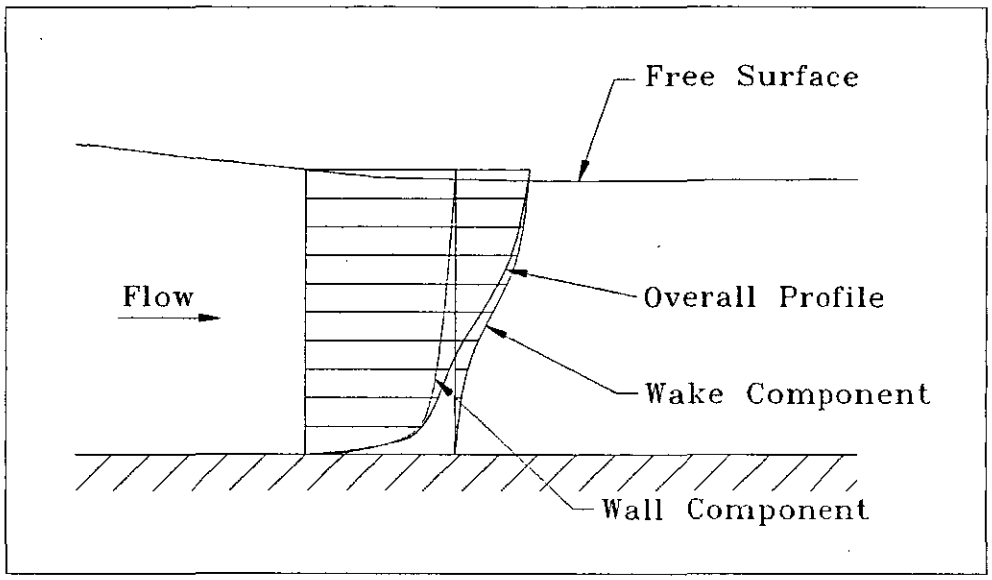

Figure 3.2.3 - Components of the Velocity Profile

3.3 Longitudinal Pressure Gradients

As shown by Chanson [3], the pressure distributions in certain regions of the undular hydraulic jump are not hydrostatic and change between vertical sections. These pressure differentials are termed longitudinal pressure gradients and were a focus of the experiments conducted. According to Kironoto and Graf [9], longitudinal pressure gradients, changes in which affect the size of the wake term, actually define the slope of the free surface.

$$\frac{\partial p}{\partial x} = \gamma\left(-S_0 + \frac{dD}{dx}\right) \tag{3.3.1}$$

where $\frac{\partial p}{\partial x}$ is the pressure gradient, $\frac{dD}{dx}$ is the water slope and S_0 is the channel slope.

Since the channel slope, S_0, in the current experiments was smaller than $\frac{dD}{dx}$, it can be said that

$$\frac{\partial p}{\partial x} \cong \gamma \frac{dD}{dx} \tag{3.3.2}$$

The non-dimensional pressure gradient is defined by Kironoto and Graf as

$$\beta = \frac{D}{\tau_0} \frac{\partial p}{\partial x} \tag{3.3.3}$$

Using the definition of v^* (equation 3.2.1) and the approximation for the pressure gradient (3.3.2) and rearranging,

$$\beta = \frac{D}{\tau_0} \gamma \frac{dD}{dx}$$

$$= \frac{D}{\rho v^{*2}} \gamma \frac{dD}{dx}$$

$$\Rightarrow \beta = \frac{gD}{v^{*2}} \frac{dD}{dx} \tag{3.3.4}$$

Thus, the non-dimensionalised pressure gradient can be determined from the friction velocity, the flow depth and the slope of the free surface. Equation 3.3.4 was used in the current experiments to find β.

3.4 Methods for obtaining the friction velocity

As previously mentioned, the investigation of the results with regard to the law of the wall requires a value of the friction velocity, v^*. This value is central to the analysis, and so time was spent determining it using different

methods, including that of Preston [6] and Clauser [2]. These methods have described in detail in the following sections.

Preston's method

In order to determine the value of v* at each measurement position, Preston [11] measured the fluid velocity with the pitot tube in contact with the channel floor. By dimensional reasoning, Preston proposed that the shear stress τ_0 is a function of ν, ρ, P, p_0 and d. He found this to be true for different pitot tube shapes and pressure gradients and that the equation was:

$$\log_{10}\frac{\tau_0 d^2}{4\rho\nu^2} = -1.396 + 0.875\log_{10}\left[\frac{(P-p_0)d^2}{4\rho\nu^2}\right] \qquad (3.4.1)$$

Thus, τ_0 can be determined from the measured velocity head at a point, given that the point measured lies in the region where the law of the wall (equation 3.2.4) holds. The value of v* is then calculated from the definition (equation 3.2.1).

Clauser's method

In order to estimate the skin friction from the velocity profile, Clauser [4] introduced a skin friction coefficient, c_f, where

$$c_f = 2\left(\frac{v^*}{U_{max}}\right)^2 \qquad (3.4.2)$$

The universal curve of $\frac{yv^*}{\nu}$ against $\frac{v}{v^*}$ was then transformed into a family of curves by substituting v* with the two variables c_f and U_{max}, the free stream velocity, and replotting the graph as

$$\frac{yU_{max}}{\nu} = \frac{yv^*}{\nu}\sqrt{\frac{2}{c_f}} \quad \text{versus} \quad \frac{v}{U_{max}} = \frac{v}{v^*}\sqrt{\frac{c_f}{2}}$$

The equation representing the lines on the graph is

$$\frac{v}{U_{max}} = 5.6\sqrt{\frac{c_f}{2}}\log\left(\frac{yU_{max}}{\nu}\sqrt{\frac{c_f}{2}}\right) + 4.9\sqrt{\frac{c_f}{2}} \qquad (3.4.3)$$

For each section, all points are plotted on this graph, and the value of c_f is determined by selecting the appropriate curve from the graph.

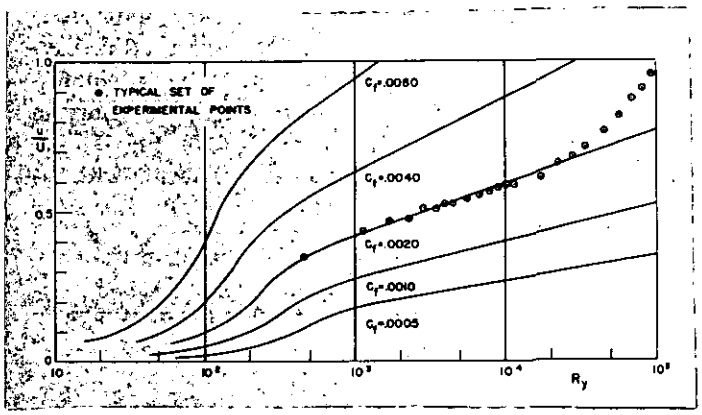

Figure 3.4.1 - Chart for Experimental Determination of Turbulent Skin Friction, Clauser [4], pp. 95

For example, the set of data plotted in Figure 3.4.1 has U_{max} = 1.0 m/s. The most appropriate value of c_f is 0.002 and therefore

$$v^* = U_{max}\sqrt{\frac{c_f}{2}} = 1\sqrt{\frac{0.002}{2}} = 0.0316\,m/s$$

A comparison of the two methods for determining v* was undertaken as part of the current experiments. For a discussion of the results, see section 6.5.

3.5 Eddy Viscosity

Another of the flow properties investigated in the undular hydraulic jump was the transport of momentum. Schubauer and Tchen [12] have suggested that the transport of momentum by turbulence may be viewed as the transport by the mean flow of a series of vortices or eddies of varying size. The eddy structure gives an indication of the amount of mixing which takes place. By analogy with laminar flow, one may define (Boussinesq [2]) an "eddy viscosity" ν_τ:

$$\tau = \rho \nu_\tau \frac{\partial u}{\partial y} \tag{3.5.1}$$

where $\frac{\partial u}{\partial y}$ = velocity gradient and τ = Reynolds shear stress.

The velocity gradient was obtained from the velocity profiles, and the Reynolds stress was assumed to vary linearly from zero at the free surface to the value $\tau_0 = \rho v^{*2}$ at the wall. The eddy viscosity is non-dimensionalised by dividing by $v^*\delta$ and is usually shown plotted against y/δ. The size of the eddies are restricted by the boundaries of the flow, the wall and the free surface.

4 Experimental Apparatus and Execution

4.1 Choice of Apparatus

Choice of the apparatus used in these experiments was based on an examination of that used in previous investigations into the undular hydraulic jump. Chanson [3] used a rectangular channel and a pitot-static tube for his measurements, and this approach was followed for the current investigations.

Modification to this design was made in consultation with Montes (pers. com.). These included the use of separate pitot and static tubes. This was for two reasons. Firstly, the tubes were fabricated specifically for the experiments and it was easier to make two separate tubes. Secondly, because of the longitudinal pressure gradients it was desired to measure the pitot and static heads at exactly the same point, which is not accomplished by combining the two tubes in the one instrument.

Another modification on Chanson's setup at the suggestion of Montes was fitting a 20 mm tapered fin on the downstream side of the vertical stem of both measuring tubes. (see Figure 4.1.1) The purpose of this was to minimise the disturbance to the flow caused by the tubes. This gave the stems a foil-like shape, greatly reducing the turbulent wake.

A gate was used to create super-critical conditions at the channel mouth (see description in 4.2).

Photo of pitot and static tubes

Figure 4.1.1 - Pitot and Static Tubes Used

4.2 Channel description

All experiments were conducted in a perspex channel with uniform rectangular cross-section having a length of 12 m, width b of 300 mm and sidewall height of 450 mm. Both the walls and bed were constructed from perspex panels 1.8 m long. (See Figure 4.2.1)

The channel was supported by a truss, spanning between a hinge support at the upstream end and a geared lifting mechanism located 7 metres downstream. This allowed adjustment of the channel slope.

Water supply was from a constant head, pump fed tank. A two-dimensional bell mouth transition was used at the inlet of the channel. Water flow was regulated by a valve positioned between the pump and the header tank inlet.

Downstream water levels were controlled by a hinged section of the bed, 400 mm long, which could be raised or lowered at the downstream end.

Critical flow conditions were obtained upstream by means of a plane gate, consisting of a single sheet of perspex wedged between the sidewalls of the channel. It was possible to vary both the gate opening and angle.

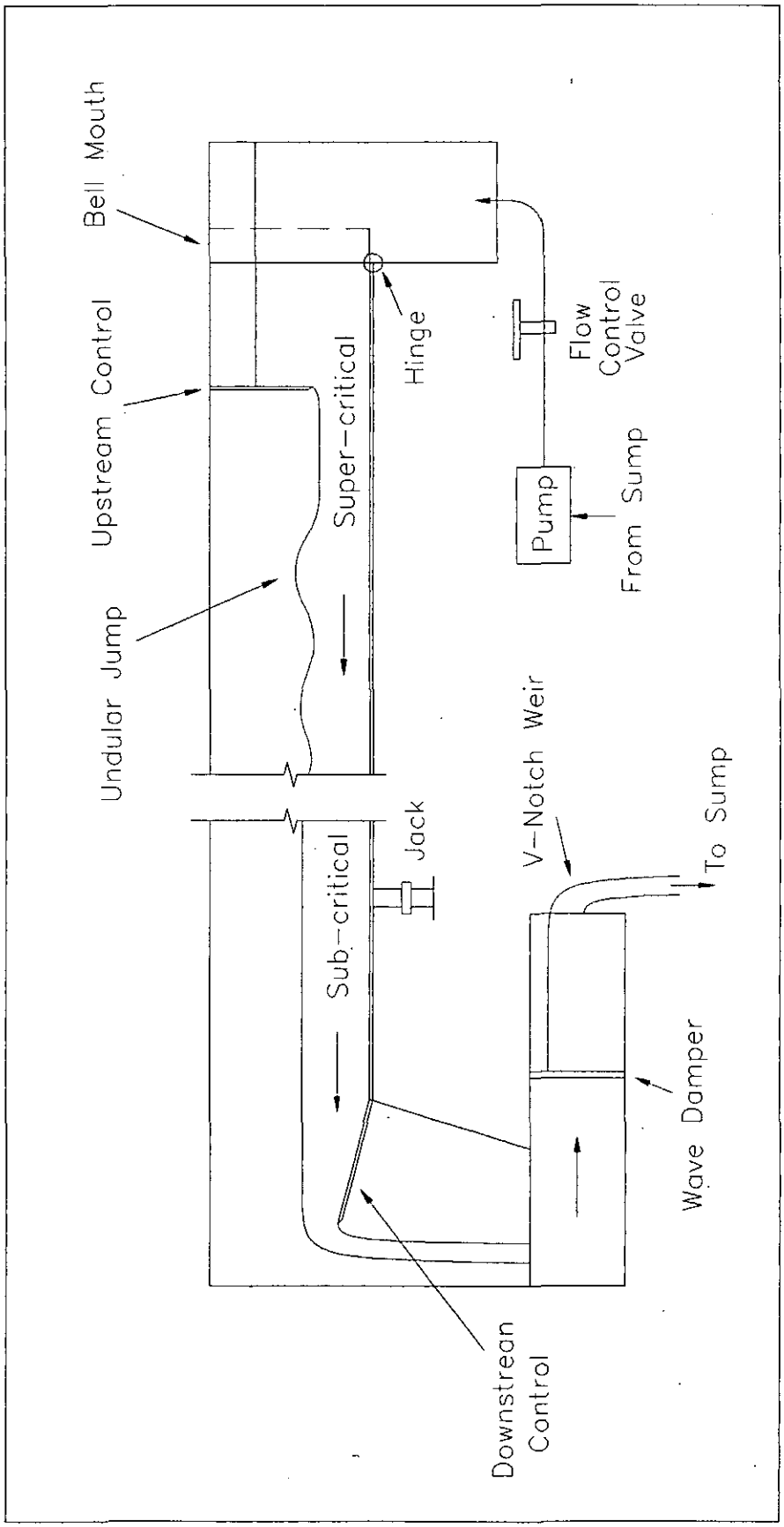

Figure 4.2.1 - Channel Layout

4.3 Instrumentation

The water discharge was measured using a 90° V-notch weir, placed at the outlet of the tank into which the channel discharged. This tank was divided into two by a permeable wall in order to dampen surface disturbances. The discharge-head (Q-h) relationship of a 90° weir has been determined by Addison [1] (in imperial units) to be

$$Q = 2.48h^{2.48}$$

which, when converted to S.I. units, can be written as

$$Q = \frac{0.309h^2}{h^{0.02}}\sqrt{2gh} \qquad (4.2.1)$$

Static head measurements were taken using a rail-mounted traveling static tube of 2.5 mm outside and 2.0 mm inside diameter. The distance between the tip and the lateral pressure holes (of 1.0 mm diameter) was 8 mm. Total head measurements were obtained using a pitot tube, also rail mounted, of 3.0 mm outside and 2.5 mm inside diameter.

The pitot and static tubes were restrained from lateral movement and were positioned in the centre of the channel. Up or downstream movement of both tubes was allowed and measured by a tape attached to the channel wall to 1 mm accuracy. Vertical height was measured by a scale fitted to the stem and was accurate to 0.5 mm

The head levels were read from a vertical manometer connected to the pitot and static tubes by 2.5 metres of nylon tubing (Nylex™ : outside diameter 9.0 mm, inside diameter 6.0 mm). At the entry to the manometer, a 70 mm section of similar, smaller tubing (outside diameter 2.5 mm, inside diameter 1.5 mm) was used do provide damping. Both manometer tubes were open to the atmosphere and had scales graduated at 1 mm intervals. The Bernoulli

equation (Gerhart and Gross [8]) was used to determine the pressure from the static head reading

$$H_{static} = z_{datum} + y + \frac{p}{\rho g} \tag{4.2.2}$$

and similarly the velocity from the total head reading from the pitot tube:

$$H_{total} = z_{datum} + y + \frac{p}{\rho g} + \frac{v^2}{2g} \tag{4.2.3}$$

4.4 Experimental Methods

The undular jumps were created using an upstream control gate placed near the channel entrance. Because of the length of the channel (12 m), long settlement times were required to obtain steady state conditions. In order to obtain an undular hydraulic jump of the required upstream Froude number, a standard method of setting up a jump was determined and is given below.

1) Set up a steady flow with a shallow slope and measure the flow rate per unit width, q.

2) Insert the upstream control gate.

3) Adjust the gate opening to give the required upstream depth for the given Froude number. The depth is derived from rearranging equation 3.1.3 to be

$$d = \sqrt[3]{\frac{q^2}{Fr^2 g}} \tag{4.4.1}$$

4) Change the level of downstream control gate to move the jump up or downstream.

5) If jump still does not form properly, change the channel slope or flow rate.

Once a stable jump was formed, measurement of the pressure and velocity distributions were made. All profiles were taken on the centre-line of the channel. For regularity, the measurements were taken relative to the position of the start of the shock waves, the crests and troughs. The positions adopted were the same as those used by Chanson [3], and are shown in Figure 4.4.1.

Points have been described using the distance before the first crest, x, as a variable. For example, x=+60 corresponds to a section taken 60 mm upstream of the first crest. Points coinciding with the crests, troughs and start of the shock waves are also labeled as shown:

Start of the first shock wave	1SW
First crest	1C
First trough	1T
Second crest	2C

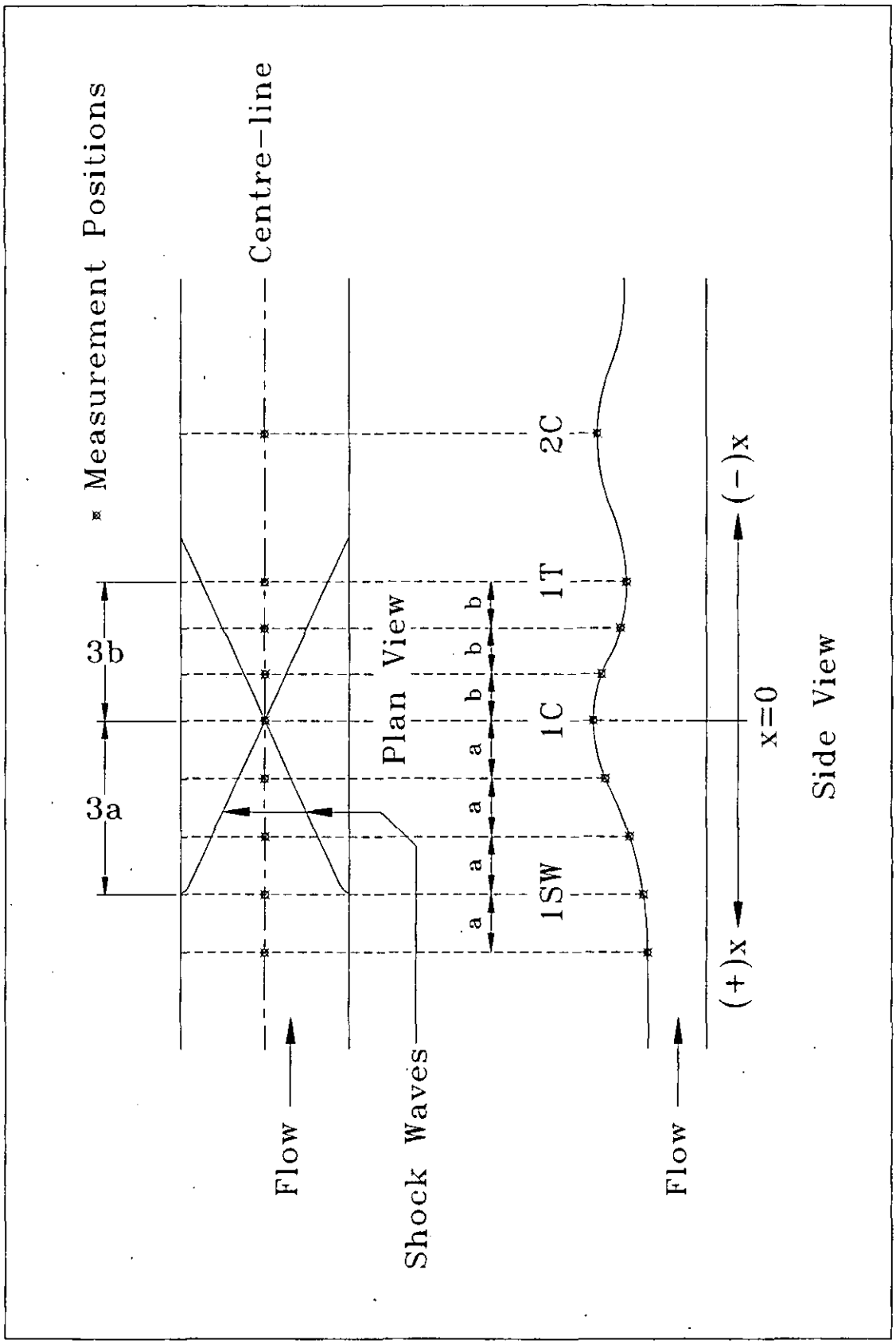

Figure 4.4.1 - Measurement Positions relative to the Jump

5 Results

The range of upstream Froude numbers for undular hydraulic jumps which could be satisfactorily measured using this apparatus, was determined before the analysis was undertaken. The minimum Froude number required for the upstream gate to produce steady, super-critical conditions was 1.4 and above 1.7, fluctuations of the manometer readings became greater than ± 5 mm, making results unreliable.

Three different jumps were set up and measurements taken. The upstream Froude numbers of the jumps were 1.41, 1.52 and 1.63. Measurements of the distribution of static and total head were made at a number of sections for each undular jump and from these, the following results were obtained. Appendix A gives a full listing of raw data, calculated values and graphs.

5.1 Pressure Distributions

Point pressures were obtained directly from the measured static head values. The pressure distributions for the three different jumps are presented in Figure 5.1.1 a) to c). The data has been plotted non-dimensionally, with the axes being the point pressure divided by the hydrostatic pressure at that point ($P/\rho gd$) and the fraction of total depth (y/d). All profiles measured for a particular jump were plotted on the same graph. A line representing a hydrostatic pressure distribution has also been included for reference.

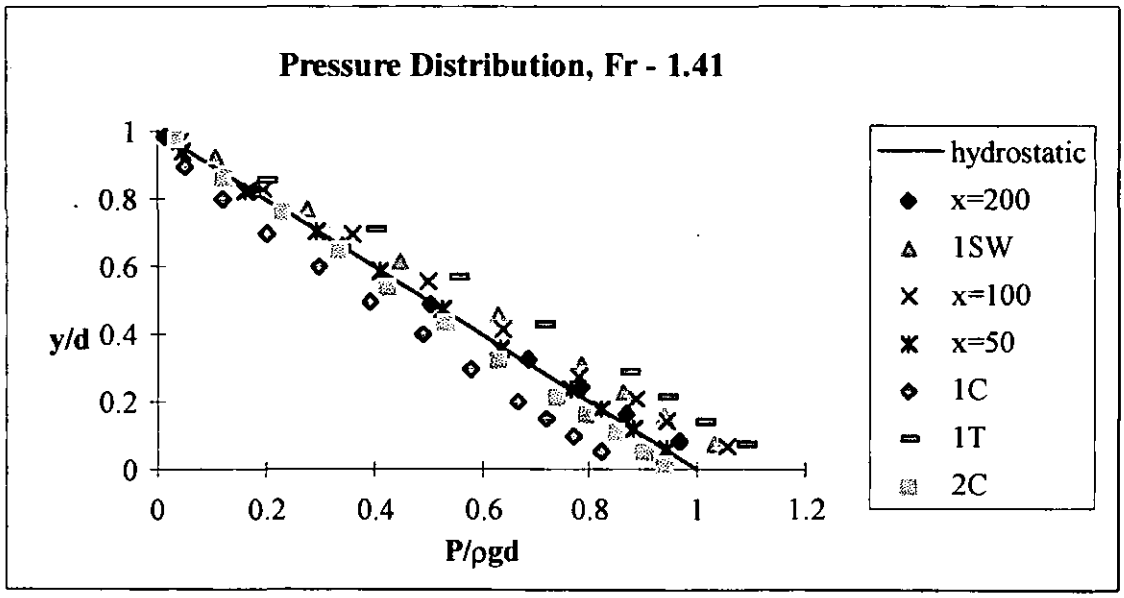

Figure 5.1.1 a) - Pressure Distributions for Upstream Froude Number = 1.41

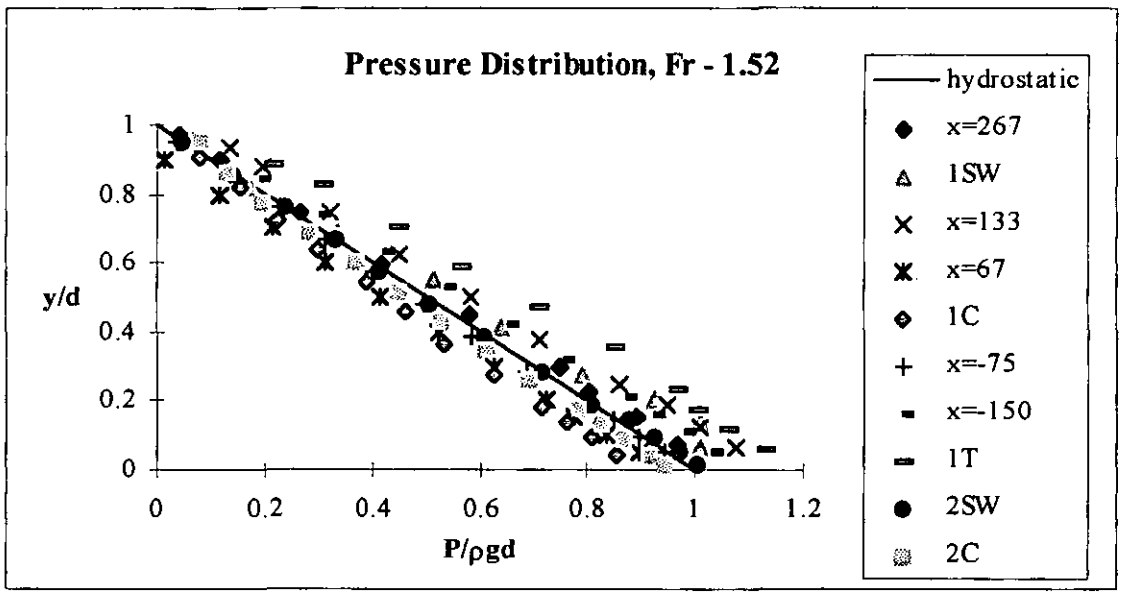

Figure 5.1.2 b) - Pressure Distributions for Upstream Froude Number = 1.52

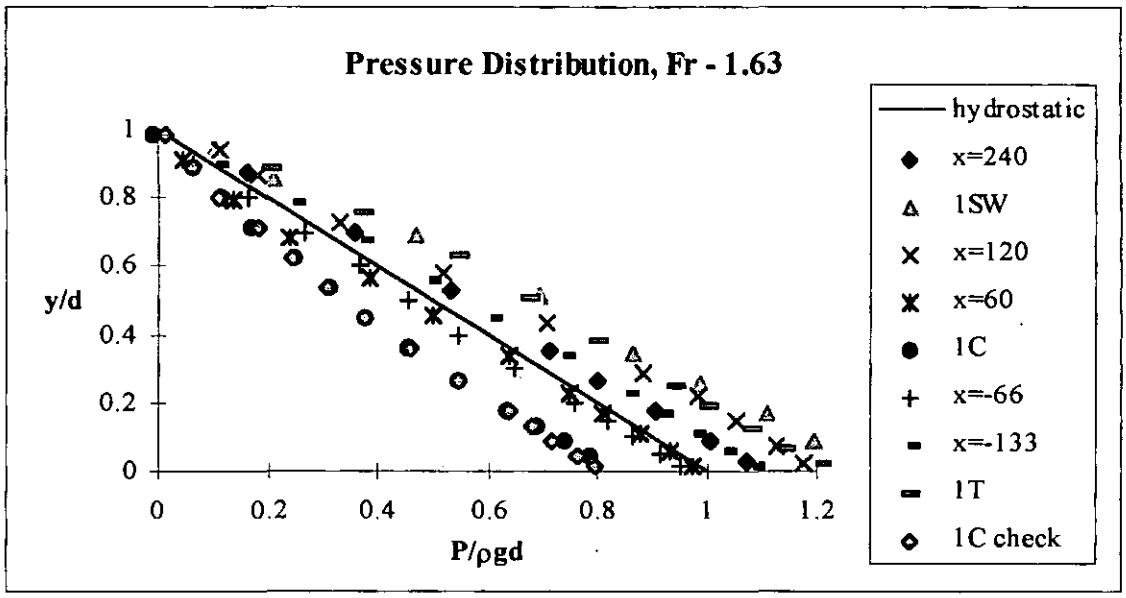

Figure 5.1.3 c) - Pressure Distributions for Upstream Froude Number = 1.63

5.2 Velocity Profiles

The difference between the total and static head yields the point velocity. Figure 5.2.1 a) to c) show the velocity profiles for each jump examined. The results are plotted non-dimensionally, with the point velocities shown as a fraction of the critical velocity (v/v_c) against the fraction of total depth at the section (y/d). The critical velocity (see Theory section 3.1) is constant for each jump Froude number.

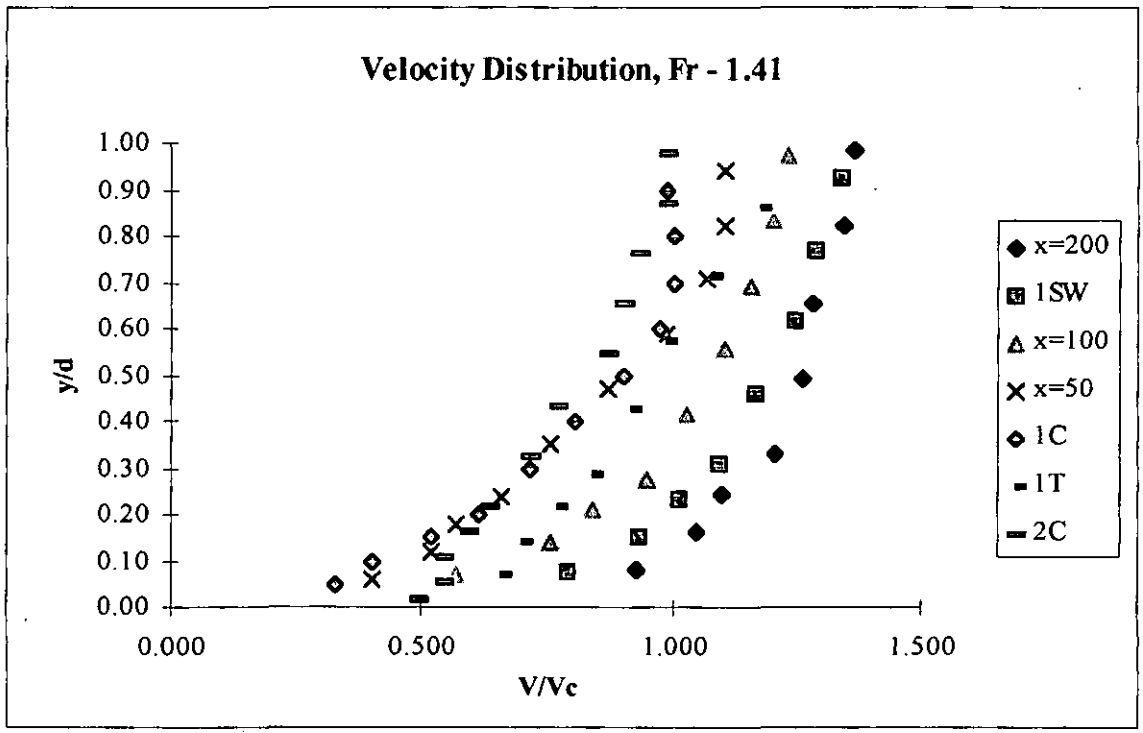

Figure 5.2.1 a) - Velocity Distributions for Upstream Froude Number = 1.41

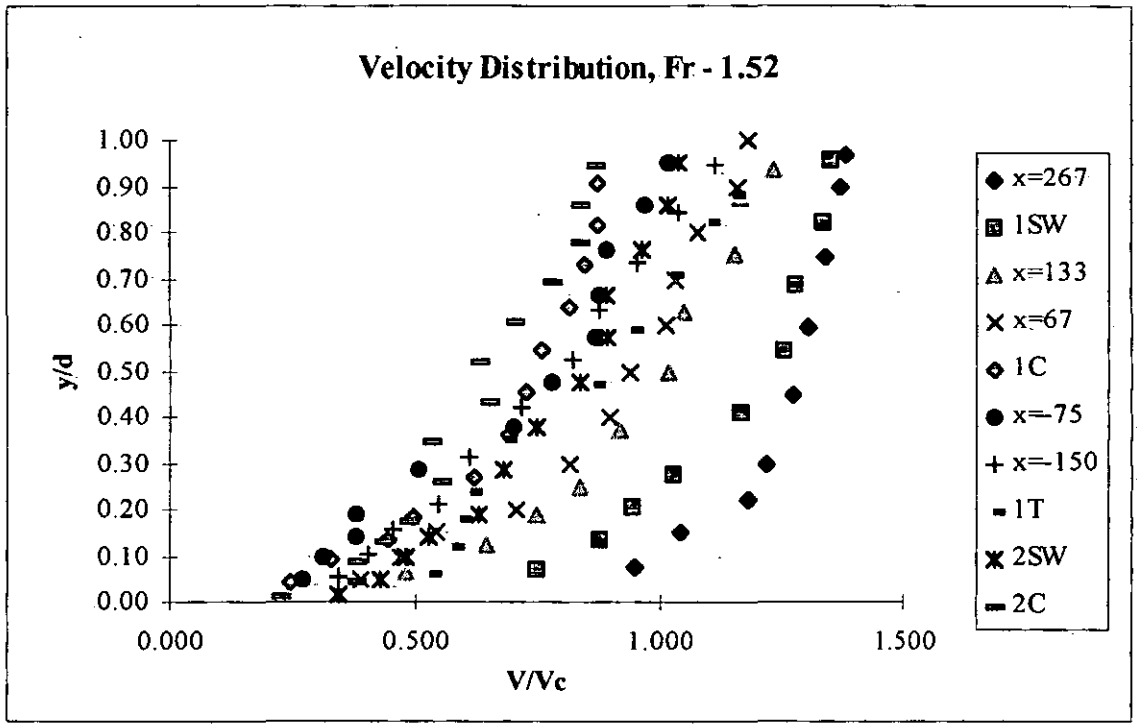

Figure 5.2.2 b) - Velocity Distributions for Upstream Froude Number = 1.52

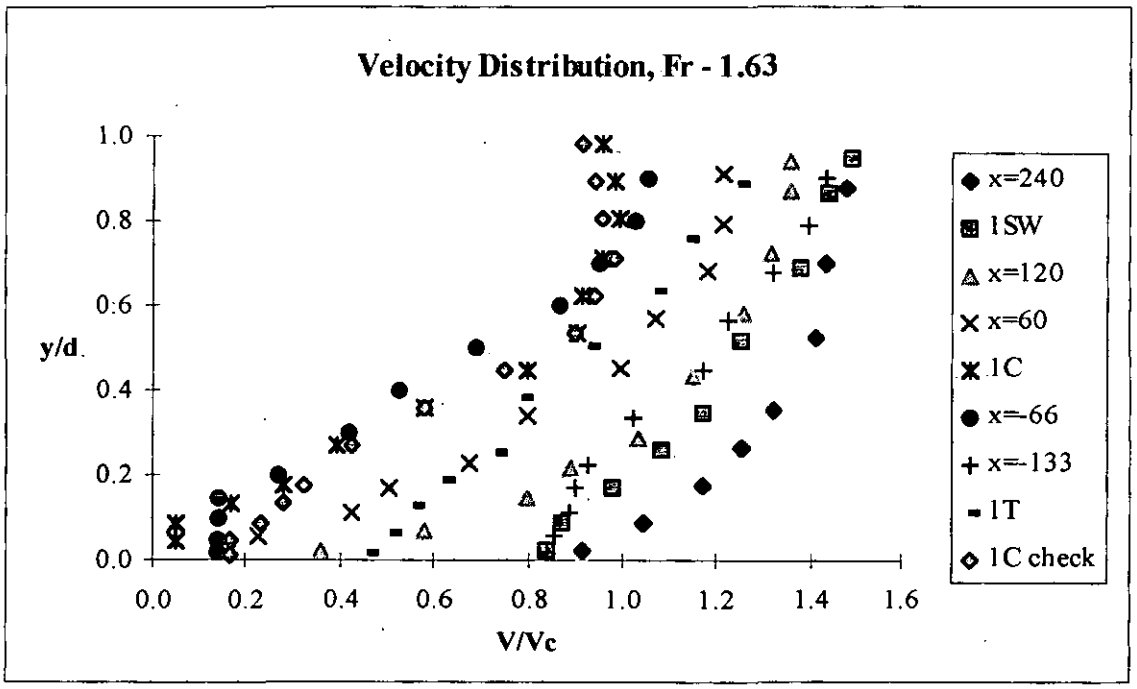

Figure 5.2.3 c) - Velocity Distributions for Upstream Froude Number = 1.63

The velocity distributions were also plotted in logarithmic form (Figure 5.2.4 a) to c)), to indicate the resemblance to that predicted by the law of the wall (see Theory section 4.2). The plot axes are of yv^*/ν against v/v^*. A line representing the theoretical law of the wall has also been plotted, the equation for which is:

$$\frac{v}{v^*} = \frac{1}{\kappa}\log\left(\frac{yv^*}{\nu}\right) + 5.1 \qquad \text{where } \kappa = \text{constant} = 0.4 \qquad (5.2.1)$$

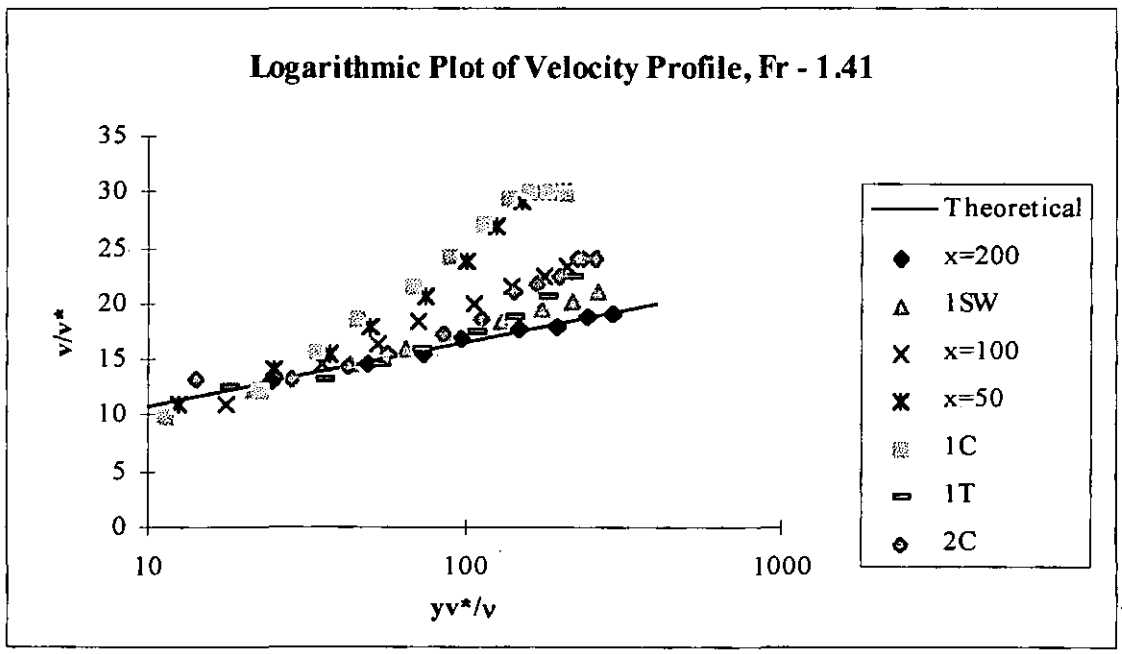

Figure 5.2.4 a) - Velocity Distributions for Upstream Froude Number = 1.41

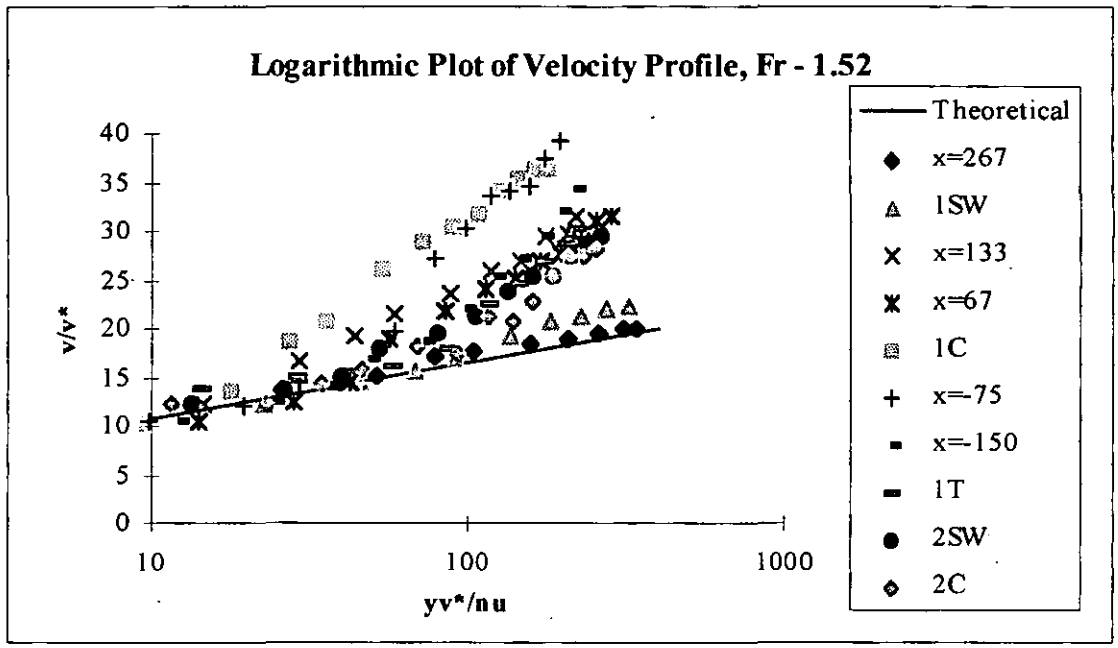

Figure 5.2.5 b) - Velocity Distributions for Upstream Froude Number = 1.52

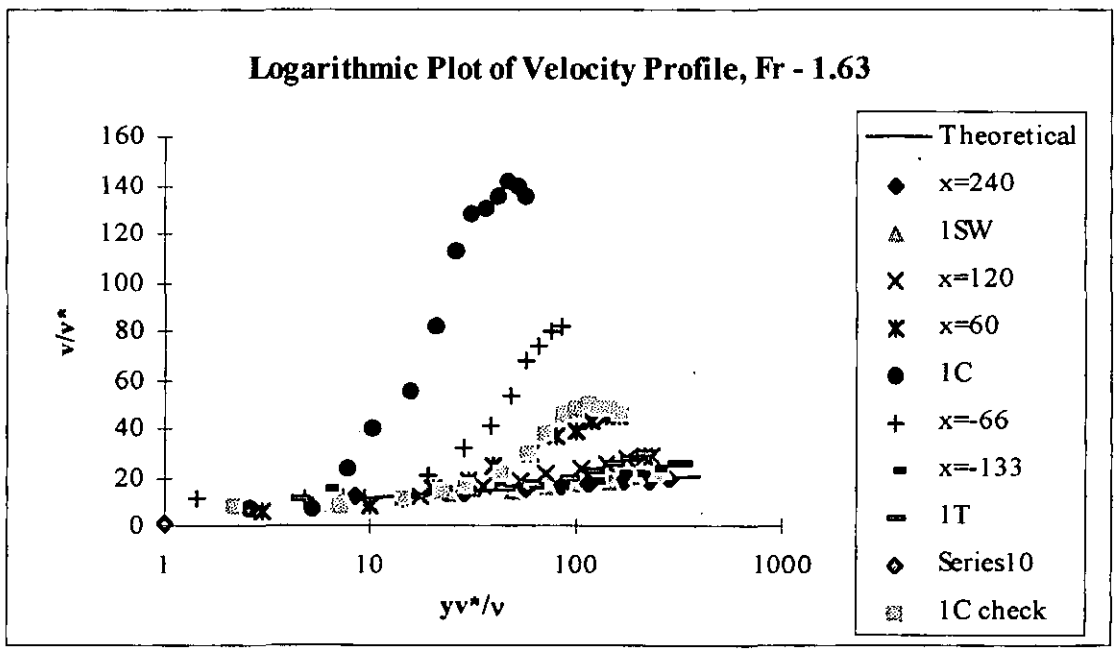

Figure 5.2.6 c) - Velocity Distributions for Upstream Froude Number = 1.63

5.3 Friction Velocity

Central to the analysis of velocity was an accurate value of the friction velocity. Detailed investigation was carried out into the comparison of the values obtained by both Preston and Clauser's methods. Figure 5.3.1 shows the comparison for the upstream Froude number of 1.52.

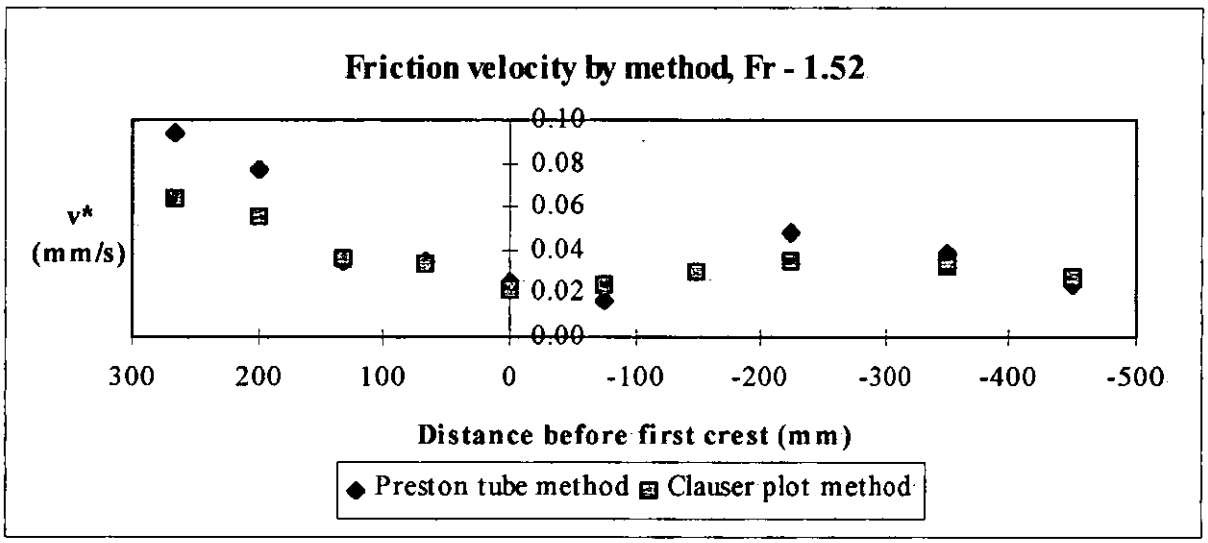

Figure 5.3.1 - Comparison of Friction Velocity measurements for Upstream Froude number = 1.52

5.4 Deviation from the Law of the Wall

Analysis of the results was carried out in accordance with Coles' theory of the law of the wake (Theory, section 4.2) to give both the shape of the wake function $\omega(y/\delta)$ and the magnitude of Coles' Π, which gives the overall size of the wake term.

Figure 5.4.1 shows the shape of the normalised wake function, ω for the case of upstream Froude number = 1.41. This was typical for all jumps. A line representing the shape of the function as determined by Coles, approximated by equation 3.2.7, has also been plotted on the graph.

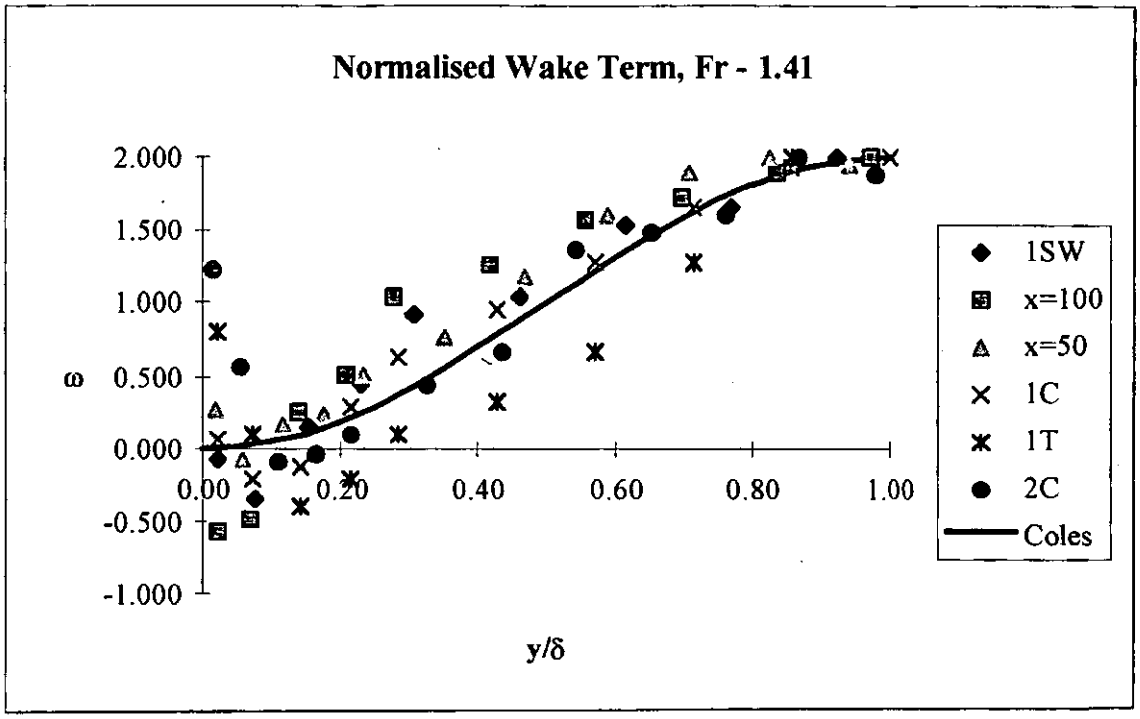

Figure 5.4.1 - Wake Function for Upstream Froude Number = 1.41

The magnitude of the wake term, as indicated by the parameter Π, showed considerable variation along the axis of the jump. This is illustrated for an upstream Froude number of 1.52 in Figure 5.4.2.

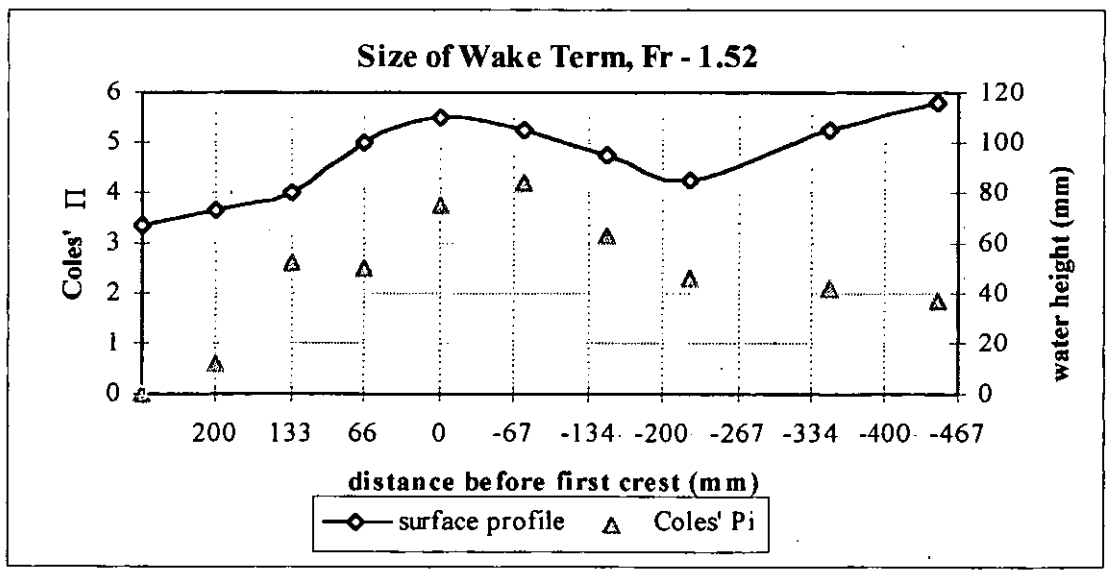

Figure 5.4.2 - Variation in size of Wake Term with Distance Along the Jump, Fr = 1.52

Variation in the size of the wake term with the longitudinal pressure gradient is illustrated in Figure 5.4.3. The data for all three jumps studied has been plotted on the one graph. The axes are the non-dimensional longnitudal pressure gradient, β (see Theory, § 4.3) against Coles' Π. All points in Figure 5.4.3 come from the region between the start of the shock waves and the first crest. The evaluation of β requires the friction velocity v*, and so points have been plotted where v* was derived using both Preston's and Clauser's method.

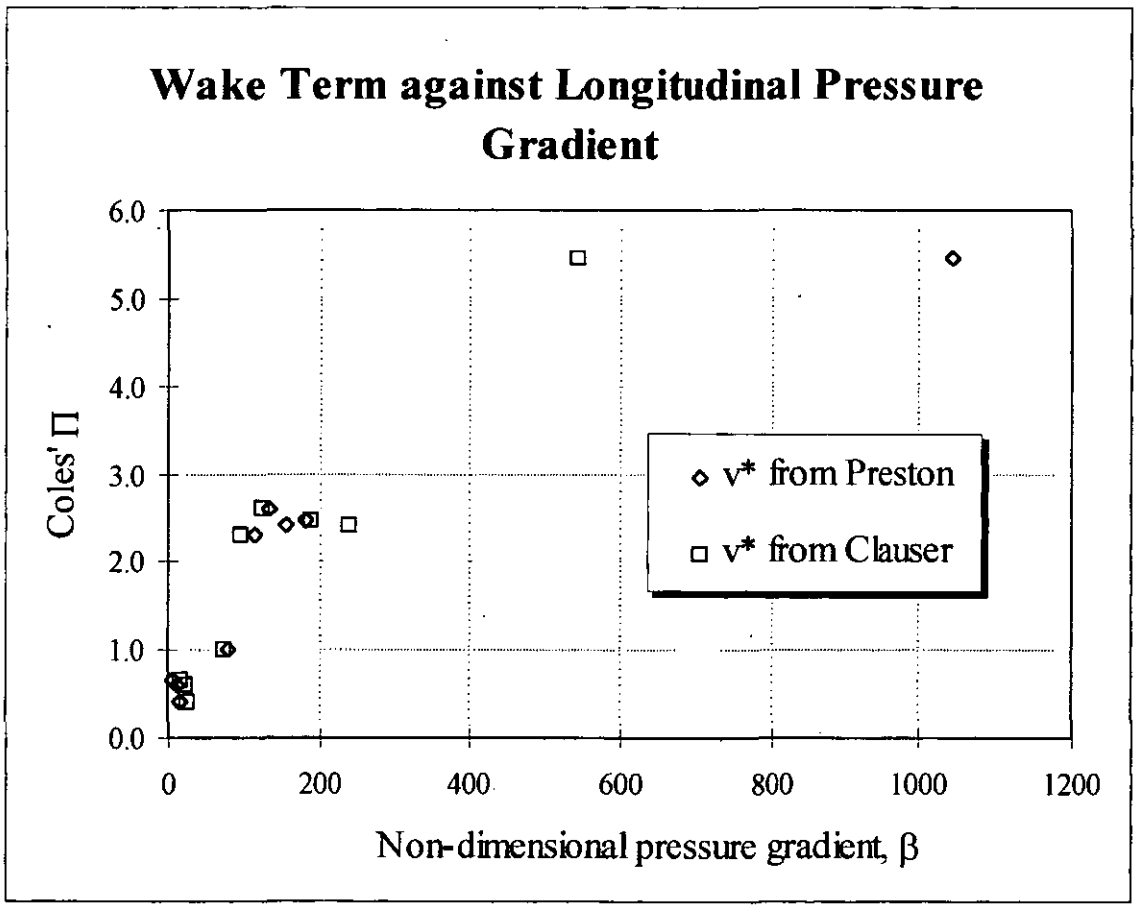

Figure 5.4.3 - Variation in size of Wake Term with Longitudinal Pressure Gradient

5.5 Eddy Viscosity

Distribution of the eddy viscosity was plotted non-dimensionally as shown in Figure 5.5.1. This plot, for an upstream Froude number of 1.41, was typical of all jumps studied. The accuracy of the points on this graph were greatly affected by the calculation of the velocity gradient, du/dy, estimated by computing the gradient between the two adjacent points on the velocity profile. Where the individual points did not lie on the average velocity profile, this method of estimating du/dy gave gross errors, so refined estimates were obtained by fitting a curve to the data using the computer program Curve Expert ®, version 1.14.

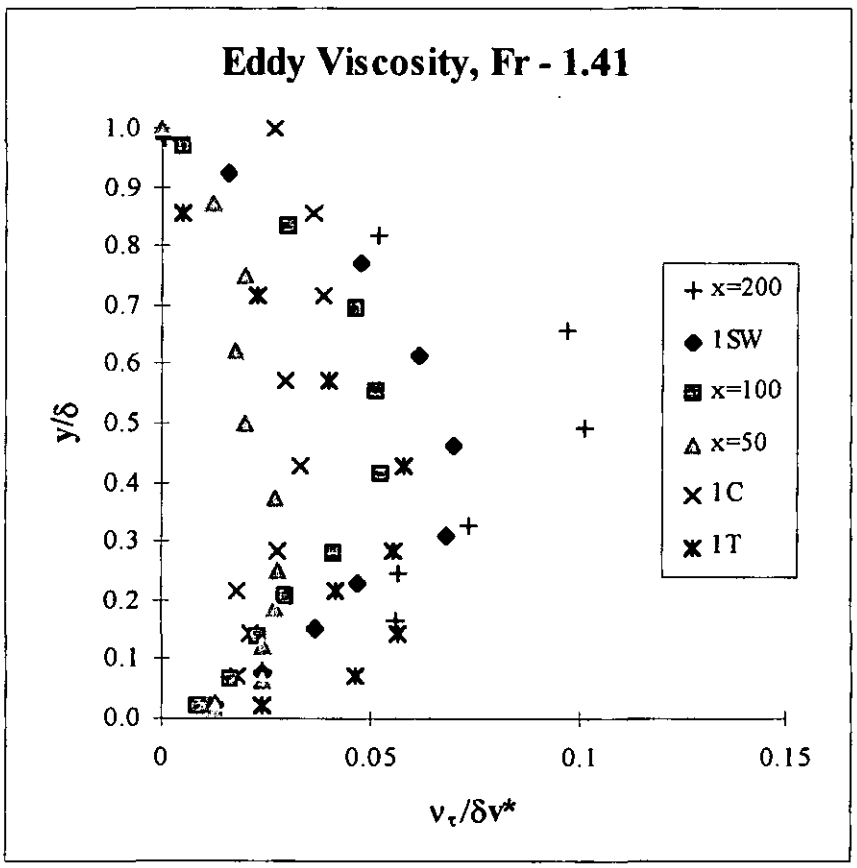

Figure 5.5.1 - Eddy Viscosity for Upstream Froude Number = 1.41

6 Discussion of Results

6.1 Pressure Distributions

It can be clearly seen in Figures 5.1.1 a) to c), that the pressure distributions within the undular jump are not hydrostatic. The deviation from hydrostatic pressure varies from - 15% at the first crest to + 15% at the first trough in all three cases. The Accuracy of individual point measurements was governed by the errors in reading the manometers. For all static head readings, variations of ± 0.5 mm of water were encountered. This represents an error of only 1 %. The effect of this small error on the results was not considered to be significant.

Other errors may have been generated due to the three-dimensional nature of the flow. Montes (pers. com.) has indicated that the velocity has a component across the channel (and thus across the static tube) at some positions within the undular jump. Duncan, Thom and Young [7] indicate that any errors are inappreciable when the flow is misaligned with the tube by up to 5%. Although this component is small, it may have resulted in the measured velocities being slightly smaller than the actual value.

6.2 Velocity Profiles

In order to illustrate how the velocity profiles change with distance along the jump, Figure 5.2.3 c) has been replotted in Figure 6.2.1, separating the velocity profiles. The upstream profiles are typical of a fully developed boundary layer. Towards the first crest, the profiles become less full and the position of the maximum velocity moves down into the flow. With the pressure reversal from the first crest to the first trough, the maximum velocity moves back to the free surface and the profiles become very flat; almost linear at the first trough. This trend from crest to trough is then repeated further downstream. Note that the profile of the jump in Figure 6.2.1 is approximately to scale.

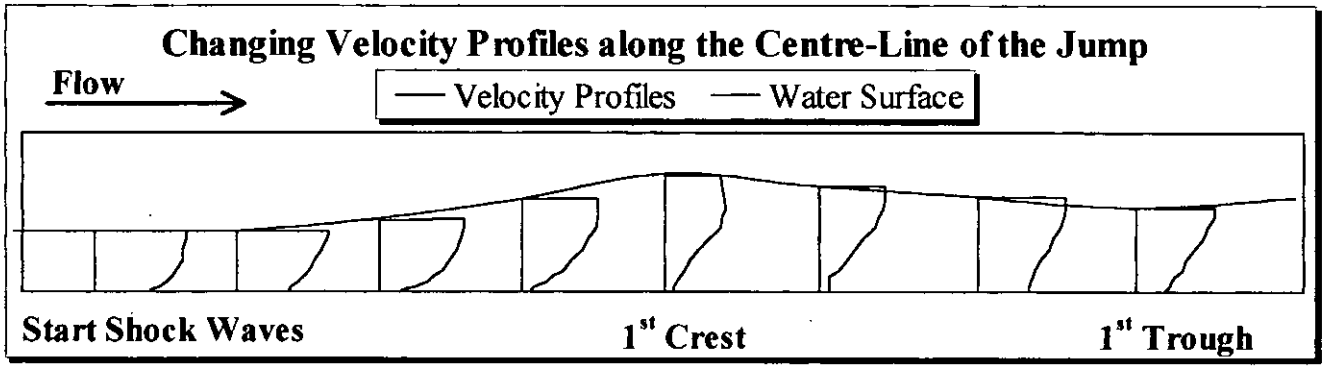

Figure 6.2.1 - Change in Velocity Profiles with Distance along the Jump

Errors in the velocities were due to the difficulty of reading the manometers. In a few highly turbulent regions of the flow, such as under the first crest, the manometer readings fluctuated by as much as ± 10 mm, however, it was possible to gain an average reading to within ± 2 mm, or about 5 %. In regions of lower turbulence, the readings obtained were accurate to ± 0.5 mm, or about 1 %. The error in the actual velocity values, when calculated from the difference between pitot and static measurements, varied depending on the proximity to the wall. As the velocities close to the wall tended to almost zero, the errors in reading the manometer values were of the order of the values actually being measured. This means that the points very near the wall were not relied upon as heavily as the other points measured for critical analytical processes. Determining the value of c_f when using Clauser's method of finding v* was such a process.

6.3 Comparison with the Results of Chanson

The results obtained from the set of experiments conducted were generally in good agreement with the work of Chanson [3]. Comparative plots of both velocity and pressure distributions on the centre line of the channel shown in Figure 6.3.1 a) and b) respectively, indicate good agreement over the range of flows investigated.

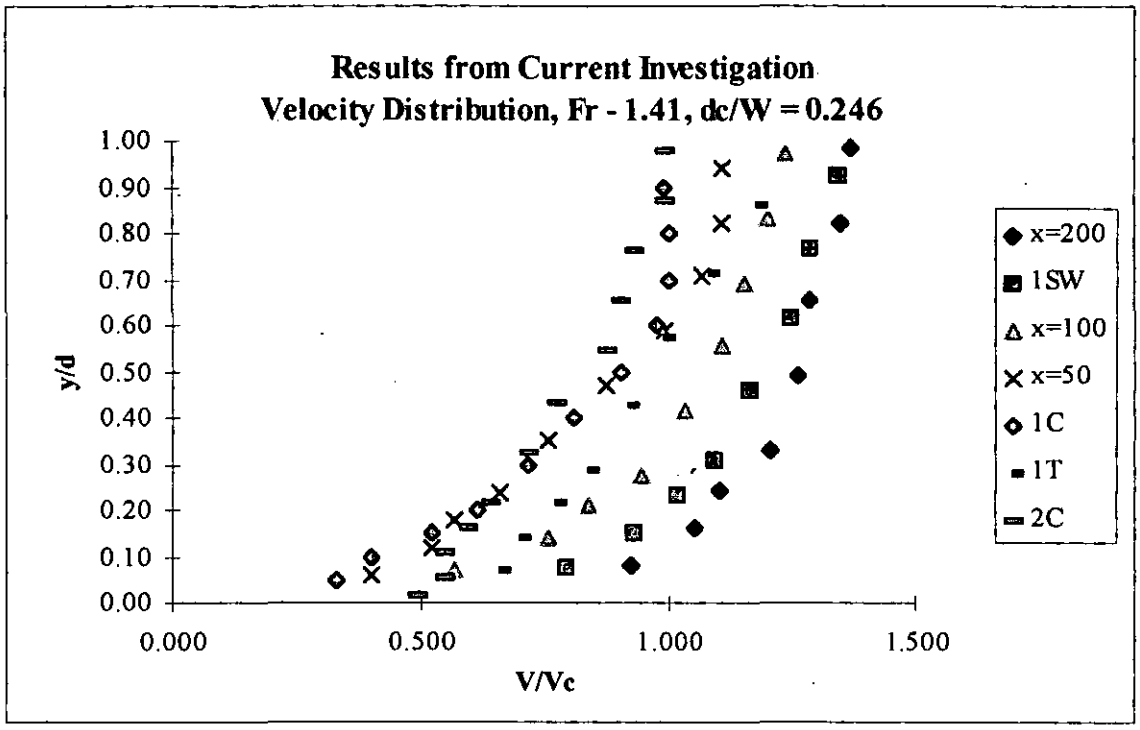

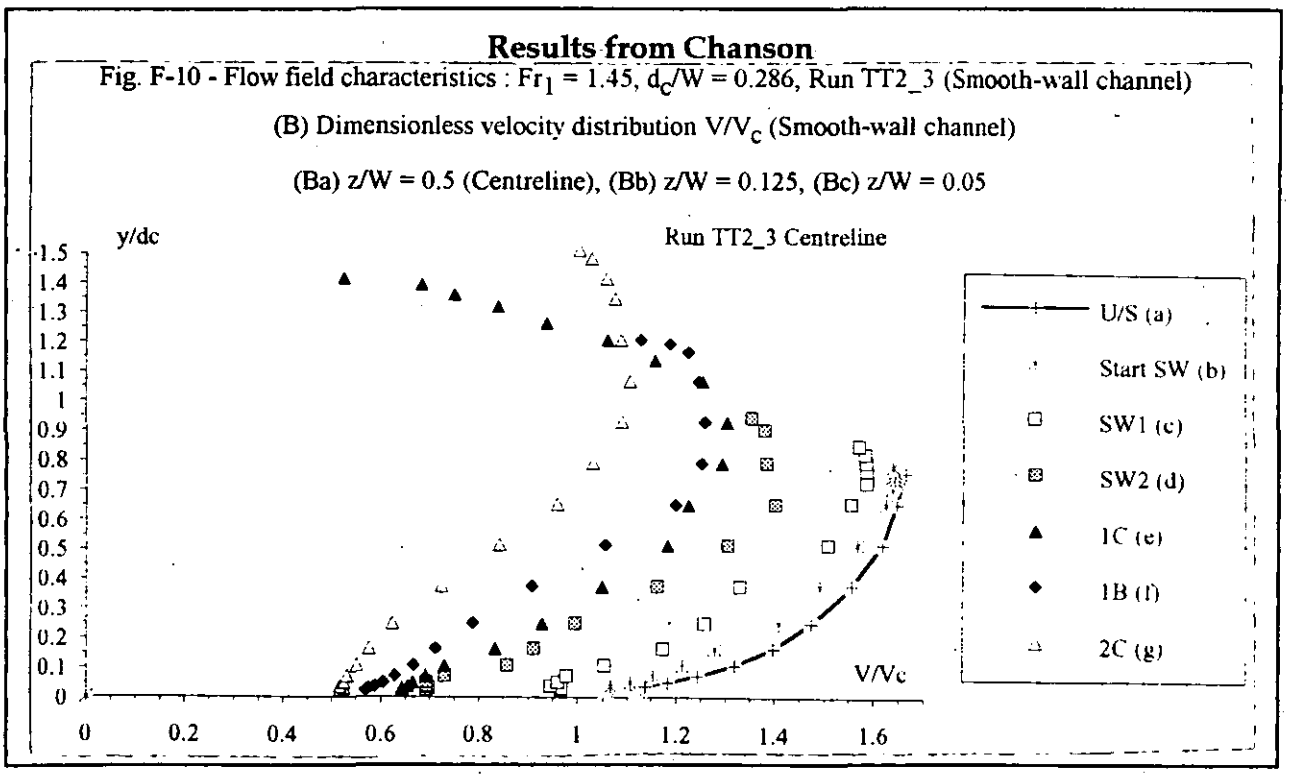

Figure 6.3.1 a) - Comparison of Velocity Profiles with Chanson

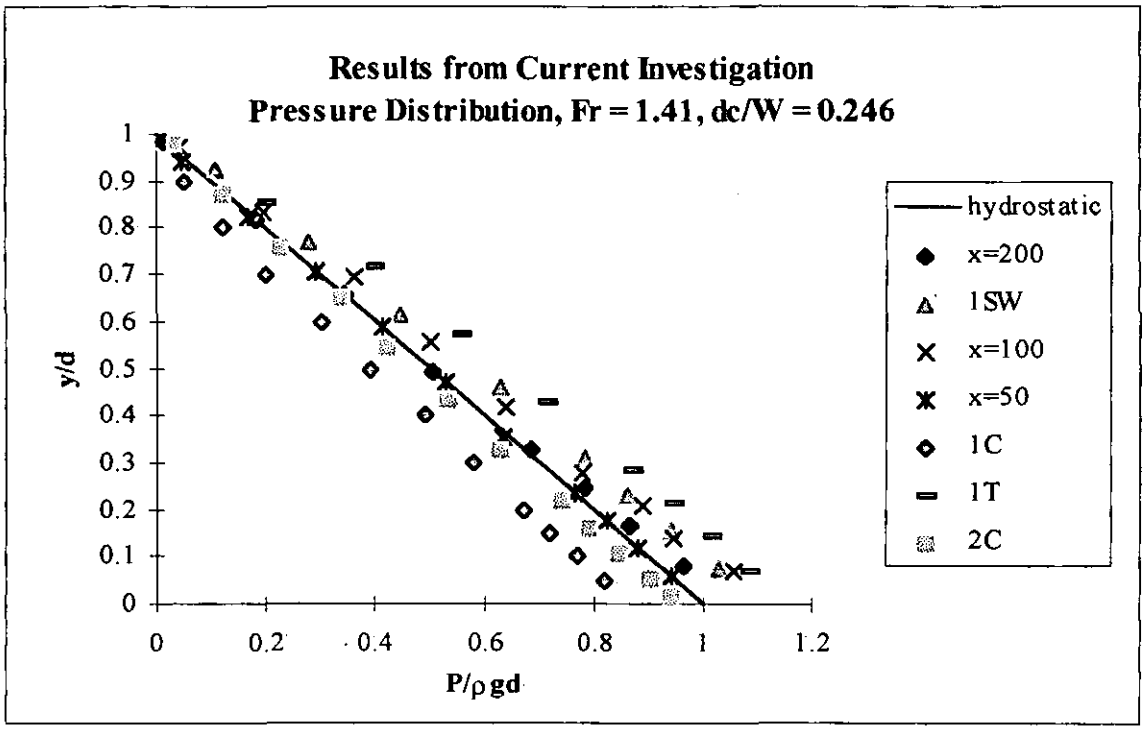

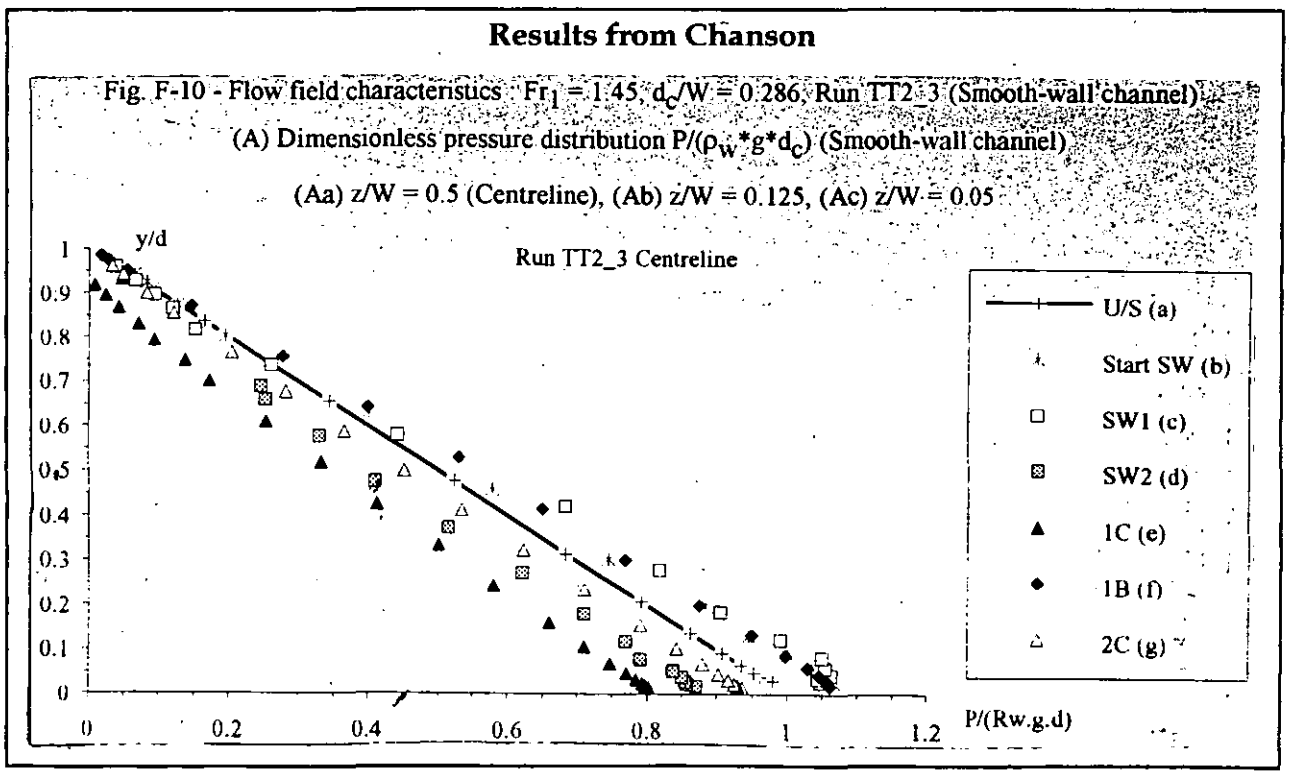

Figure 6.3.1 b) - Comparison of Pressure Distributions with Chanson

As previously described in section 4.1, the major difference between the channel setup and that of Chanson was the use of a gate to create critical flow. Chanson had relied on the flow to become fully developed before the jump, which occurred 10 to 12 metres downstream from the intake. In the current experiments, the jump formed approximately 2 metres from the gate, which itself was 2 metres from the intake. The shape of the velocity profiles measured upstream of the jump are typical of those found in fully developed flows.

Another difference between the experiments was the aspect ratio of the jump, d_c/W. As the undular jump is a three dimensional feature, this ratio may be expected to make a difference, but the similarity of the results show that the effect of this on the shape of the velocity profiles on the centre-line was apparently not great.

6.4 Comparison with the Results of Kironoto and Graf

Studies of velocity profiles in mild longitudinal pressure gradients have been undertaken by Kironoto and Graf [9]. Comparisons of my results with theirs revealed the following:

The shape of the velocity profiles were in good agreement. Regions of accelerating flow correspond to the peaks, where the peak velocities were below the free surface, while decelerating regions corresponded to troughs, with very flat profiles. Profiles from the undular jump revealed less difference between the maximum and surface velocities. This may have been due to the high pressure gradients, or because of the difference in Froude numbers ($Fr \approx 1.0$ for the current experiments as opposed to $Fr \approx 0.3$)

6.5 Measurement of the Friction Velocity

Obtaining a value for the friction velocity, v* at each cross section was an important step in the analysis of the results. Slight changes in v* shifted the points on the logarithmic plot of the velocity profiles since it is included in both axes. A 10% increase in the value of v* can make a very noticeable difference as seen in Figure 6.5.1.

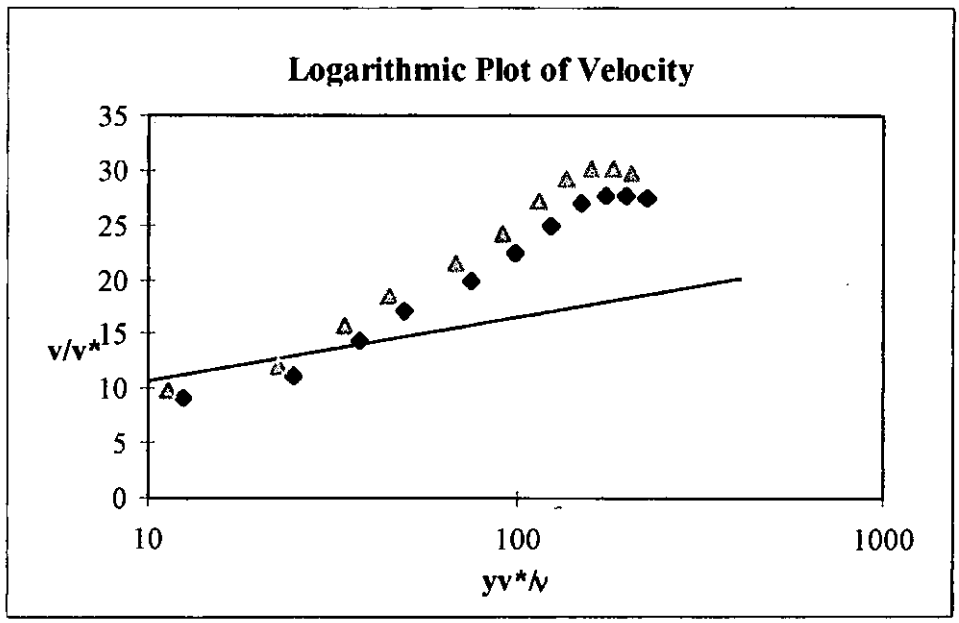

Figure 6.5.1 - Illustration Showing how a 10% Change in v* Shifts the Velocity Profile on a Logarithmic Plot.

Two different methods for determining the friction velocity were undertaken. The change in thickness of the boundary layer along the jump varied substantially, particularly under the first crest where recirculation occurred and under troughs where it was greatly reduced. This made Preston's method more difficult to use accurately, because it requires measurement at discrete points. Clauser's plot method uses the description of the whole velocity profile to determine a value for the friction velocity. Where the two methods differed greatly, this method also gave more favorable results with respect to the position of the velocity points on the logarithmic plot, and their correlation to the law of the wall. Variations in the values of v* calculated by

the different methods were up to 20 % as can be seen in Figure 5.3.1 (results section).

6.6 Law of the Wall and Law of the Wake

The analysis of the velocity profiles was done in relation to current theory for zero pressure gradients, the law of the wall, and theory for flows in longitudinal pressure gradients, Coles' law of the wake.

Measurements indicate (Figure 5.2.4 a) to c)) that the logarithmic relationship between v/v^* and yv^*/ν was followed for the regions of flow immediately before the jump where the pressure gradient is small. The data fitted well to equation.3.2.4, with the constants for the being

$$A = 2.5$$
$$B = 5.1$$

Deviation from this relationship was observed for most of the sections at which the measurements were taken. Deviations became noticeable downstream from the start of the shock waves, with only one or two points of these profiles adhering to the law of the wall.

This deviation from the law of the wall was analysed with respect to the wake function and it can be seen from Figure 5.4.1 (Results section) that it is representative of Coles' typical function $\omega(y/d)$.

The section measured at the position immediately before the first crest indicated that the flow had began to deviate from the logarithmic relationship and remained so for all measurements downstream of this position. Comparison to Coles' wake function was undertaken for all positions aforementioned (see Figure 5.4.1). It is quite noticeable that the wake functions measured between the position immediately before the first crest and the first trough tend to lie above the function proposed by Coles, although they have a similar S-shape.

6.7 The Effect of the Pressure Gradient

The definition the non-dimensional longitudinal pressure gradient parameter, β, as seen in section 3.3, involved the slope of the free surface. For the range of Froude numbers of the jumps investigated, the relative height of the first crest is high and the water surface slope is large. Because of this, the magnitude of the longitudinal pressure gradient was expected to be quite large also. Measurements revealed this to be true, with β ranging up to 1000.

The variation of β along the jump was governed by the size of the free surface gradient, as the term δ/τ_0 was significantly less than dp/dx. Hence, the pressure gradients varied from zero before the jump to a maximum positive before the first crest through another zero at the first crest to a maximum negative before the first trough.

The relationship between β and Coles' Π was of interest, because of the large values of β encountered in the experiments. A definite trend could be noted from the limited amount of points plotted in Figure 5.4.3. In order to investigate this further, comparison was made to data obtained from Coles and Hirst [6].

The data obtained from Coles and Hirst [6] covered a wide range of positive pressure gradients, β ranging from 0 to 2000. Figure 6.7.1 shows the results plotted in logarithmic form. The computer program Curve Expert ®, version 1.14, was used to generate curves of best fit, and it was found that a power curve of the form

$$\Pi = A\beta^B + C \qquad (6.6.1)$$

where A, B and C are constants, provided the closest correlation. The line shown in Figure 6.7.1 has the following values:

A = 0.246

B = 0.431

C = -0.03

A correlation R = 0.96.

As can be seen from this plot, the curve generally fits the whole range of data very well. However, a plot of the lower β values (normal axes), as shown in Figure 6.7.2, indicates the intercept on the Π axis should be closer to 0.2. Also, the power fit should only be applied to positive values of β, as negative values were not investigated.

The most surprising aspect to note from investigation of the size of the wake term is that a single relationship was found for the great range of flow patterns investigated. These include fully three dimensional flows (undular jump), gradually varied two dimensional flow (diffusers, diverging channel) and purely two dimensional flow (aero-foil, channel flow over step, accelerating flow). This indicates that the concept of law of the wake is indeed a very useful and universal tool for boundary layer analysis.

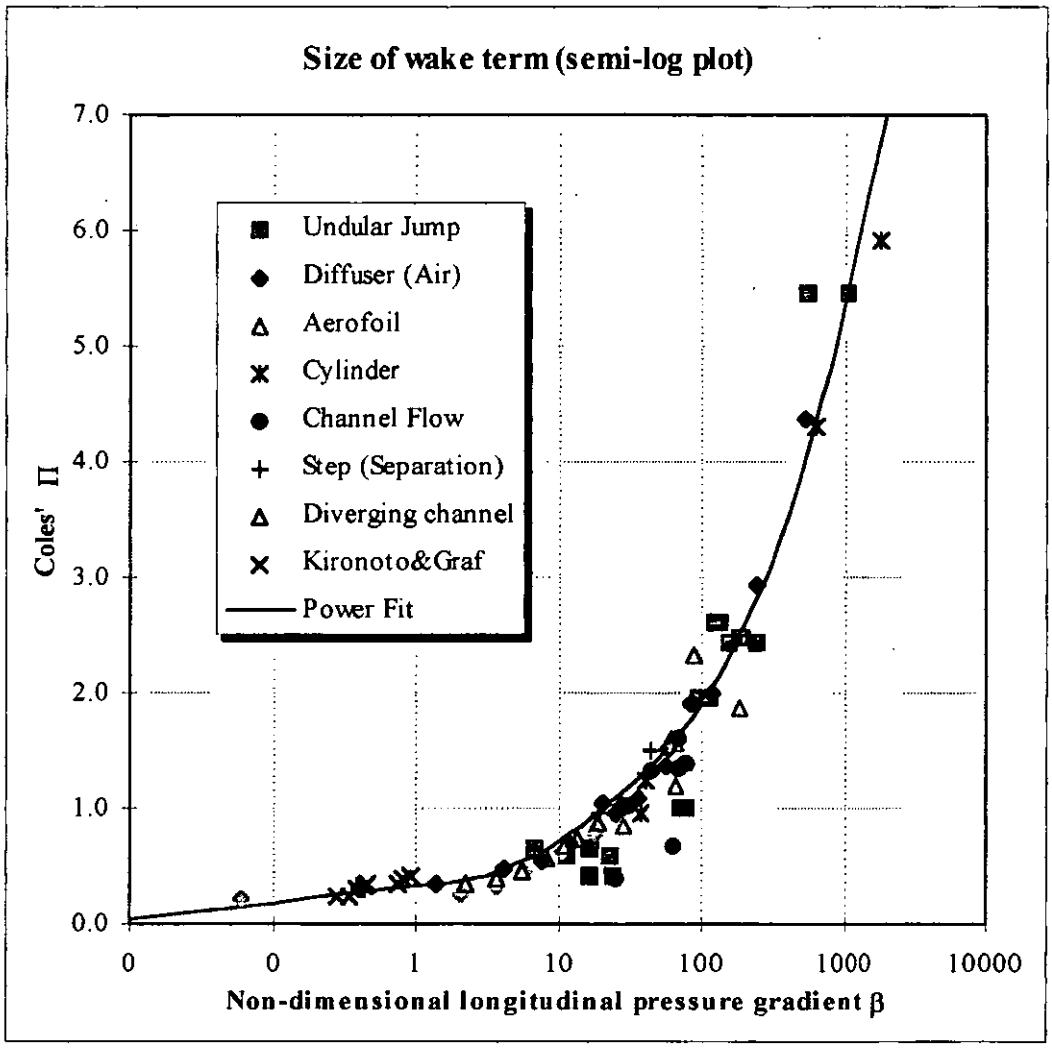

Figure 6.7.1 - Logarithmic Plot of Size of Wake Term with Longitudinal Pressure Gradient for Many flow Situations

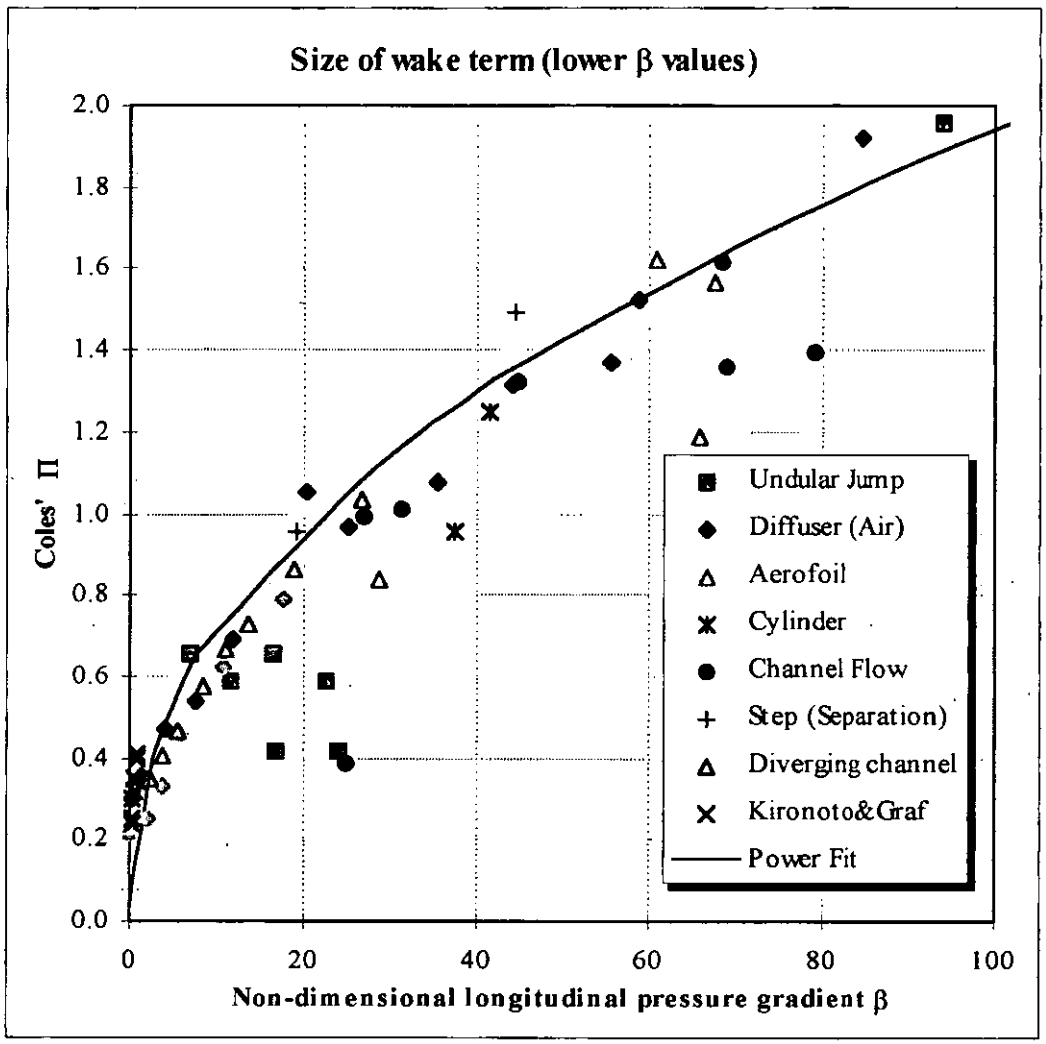

Figure 6.7.2 - Plot of Size of Wake Term with Longitudinal Pressure Gradient for Many flow Situations

6.8 Eddy Viscosity

The plot of the eddy viscosity in Figure 5.5.1 has been replotted in Figure 6.8.1 to show the comparison with those found by Kironoto and Graf [9]. Although a very limited amount of data was given in the paper, the general shapes of the eddy viscosity profiles were the same.

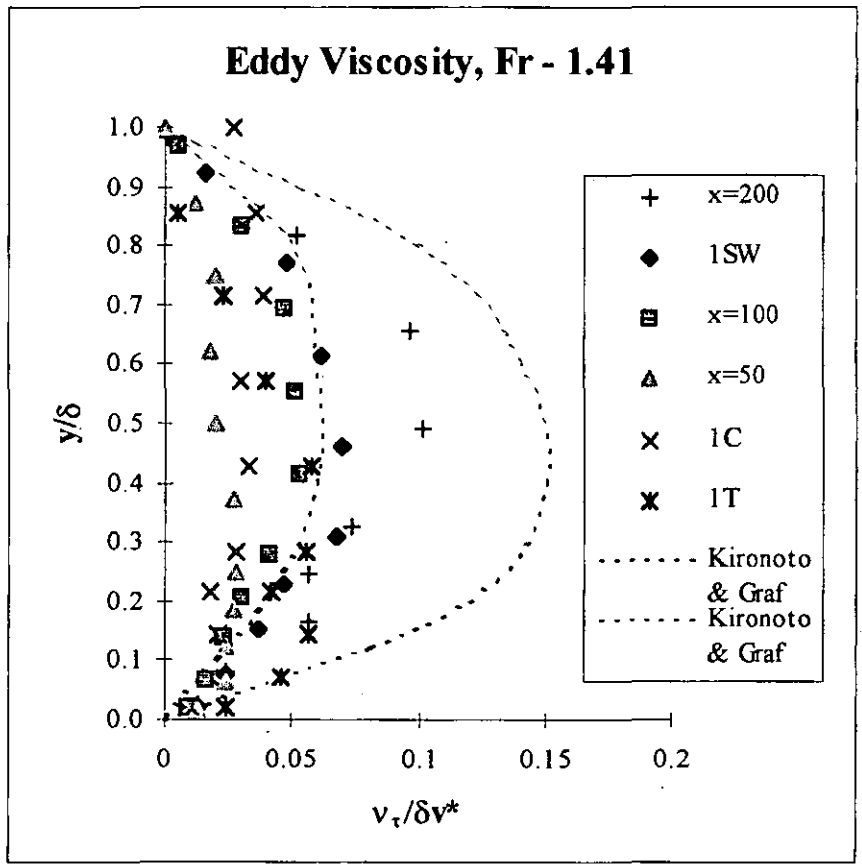

Figure 6.8.1 - Comparison of Eddy Viscosity with the Results of Kironoto and Graf [9]

The validity of these results may be somewhat doubtful, as an assumption in calculating the eddy viscosity was made as to the distribution of Reynolds' shear stress over the section. It was assumed to be linear from zero at the free surface to equal τ_0 at the wall. This assumption was not checked experimentally.

7 Conclusion

7.1 Conclusions Drawn

The conclusions which can be drawn from the current investigation can be summarised as follows:

- The formation of non-hydrostatic pressures within an undular hydraulic jump are associated with velocity profiles of great variability within relatively short distances along the jump. These variations from uniform flow values are linked to the surface curvature of the flow.

- Velocity profiles followed the accepted theories of turbulent boundary layer flow with respect to the law of the wall and the law of the wake.

- The shape of the wake function was similar to that found by Coles [5], even though the pressure gradients were much higher than the flows he investigated.

- The amount of mixing and distribution of eddy viscosity in the undular jump compared favourably with other cases of much smaller pressure gradients in open channel flow.

- A relationship between the magnitude of the wake term and the longitudinal pressure gradient was found for a wide range of pressure gradients and for different flow regimes.

- Conformity of the measurements from the undular hydraulic jump to the relationship mentioned above, suggests that further insights into the undular hydraulic jump flow may be derived from well established boundary layer development methods which have proved suitable in similar large longitudinal pressure cases.

This project has been successful in its aims to investigate the velocity profiles of the jump on the centre-line and to compare the flow regime to other flow situations.

In addition to this, the investigation into the wake term has yielded a new empirical formulation for the relationship between the size of the wake term and the longitudinal pressure gradient.

7.2 Practical Relevance

Chanson [3], has noted that the effects of undular hydraulic jumps need to be seriously considered by designers. Erosion of banks caused by overtopping, increased fatigue loads, disruption of navigation and pump operation can all be caused by undular hydraulic jumps.

The investigation into the velocity profiles conducted in this report provides useful information on the flow patterns and may be helpful in preparing an accurate model for prediction of the occurrence and effects of undular hydraulic jumps.

7.3 Future Work

The experiments performed in this project show that the flow mechanisms occurring within the undular hydraulic jump are not dissimilar to those occurring in other flow situations. However, the study was principally aimed at flow along the centre-line of the jump. As shown by Chanson [3], the flow patterns exhibit three dimensional characteristics. Further investigation of the flow in a fully three dimensional manner should be undertaken before theoretical models can be further developed.

8 References

[1]Addison, H. (1956) *A Treatise on Applied Hydraulics* Chapman & Hall, London.

[2]Boussinesq, J. V. (1871) Sur le Mouvement Permanent Varié de l'Eau dans les Tuyaux de Conduite et dans les Canaux Découverts (On the Steady Varied Flow of Water in Conduits and Open Channels) Comptes Rendus des séances de l'Académie des Sciences 73: 101-105 (in French)

[3]Chanson, H. (1995) *Flow Characteristics of Undular Hydraulic Jumps, Comparison with Near-Critical Flows* University of Queensland, Department of Civil Engineering Report CH45/95 Queensland.

[4]Clauser, F. H. (1954) Turbulent Boundary Layers in Adverse Pressure Gradients Journal of the Aeronautical Sciences 21(2): 91-108

[5]Coles, D. (1956) The Law of the Wake in the Turbulent Boundary Layer Journal of Fluid Mechanics 1(2): 191-226

[6]Coles, D. E. and Hirst, E. A. (1968) *Proceedings - Computation of Turbulent Boundary Layers AFOSR - IFP - Stanford Conference, Volume 2* Department of Mechanical Engineering Stanford University California.

[7]Duncan, W. J., Thom, A. S., and Young, A. D. (1970) *The Mechanics of Fluids* Edward Arnold London.

[8]Gerhart, P. M. and Gross, R. J. (1985) *Fundamentals of Fluid Mechanics* Addison-Wesley Massachusetts.

[9]Kironoto, B. A. and Graf, W. (1995) Turbulence Characteristics in Rough Non-uniform Open-channel Flow Proceedings of the Institution of Civil Engineers, Maritime & Energy 112: 336-348

[10]Prandtl, L. (1935) The Mechanics of Viscous Fluids Aerodynamic Theory (Durand) 3: 35-208

[11]Preston, J. H. (1954) The Determination of Turbulent Skin Friction by Means of Pitot Tubes Journal of the Royal Aeronautical Society 58: 109-121

[12]Schubauer, G. B. and Tchen, C. M. (1961) Turbulent Flow Princeton University Press New Jersey.